THE CRYSTALLIZATION OF TOUGH THERMOPLASTIC RESINS IN THE PRESENCE OF CARBON FIBERS

Grant number - NAG-1-525 S-1

A Technical Report
for the year ending December 31, 1986

submitted by

Dr. Michael H. Theil, Principal Investigator
College of Textiles
Department of Textile Chemistry
Box 8302, North Carolina State University
Raleigh, NC 27695-8302

submitted to

Dr. Noel T. Wakelyn
Technical Officer
and
Dr. Norman J. Johnston
MD M/S 226
National Aeronautics and Space Administration
Langley Research Center
Hampton, VA 23665

THE CRYSTALLIZATION OF TOUGH THERMOPLASTIC RESINS IN THE PRESENCE OF CARBON FIBERS

Grant number - NAG-1-525 S-1

A Technical Report
for the year ending December 31, 1986

submitted by

Dr. Michael H. Theil, Principal Investigator
College of Textiles
Department of Textile Chemistry
Box 8302, North Carolina State University
Raleigh, NC 27695-8302

submitted to

Dr. Noel T. Wakelyn
Technical Officer
and
Dr. Norman J. Johnston
MD M/S 226
National Aeronautics and Space Administration
Langley Research Center
Hampton, VA 23665

ACKNOWLEGDEMENT

Mr. Timothy W. Towell, a graduate student at North Carolina State University, did the experimental work described here and made major contributions to the planning of the program, the interpretation of results, and the writing of this report.

The financial and contributions of NASA's Langley Research Center, and the technical advice of its personnel are gratefully acknowledged.

ABSTRACT

The presence of carbon fibers increased the crystallization rates of both poly(aryl-ether-ether-ketone) (PEEK) and poly(phenylene sulfide) (PPS) thermoplastic polymers. The effect was most pronounced at higher crystallization temperatures. Isothermal crystallization rates were analyzed by applying classical phenomenological nucleation theory. Unusually high values of the so-called Avrami exponent were found for neat PEEK.

Isothermal crystallization of PEEK and PPS polymers produced crystalline samples having a wide variety of melting temperatures. The melting as observed by differential scanning calorimetry occurred as dual endotherms which were called primary (higher temperature) and secondary melting peaks. Each primary peak accounted for most of the crystallinity present. The secondary peaks represented the melting of crystallites formed later than those attributable to the primary endotherms. The presence of carbon fibers increased the thermal stability of both PEEK and PPS crystallites as manifested by higher temperatures for the primary melting peaks. This may be attributable to increased crystallite size, greater crystallite perfection, and/or favorable modification of the crystallite interface. Over the range studied, crystallization temperature strongly influenced the positions of the secondary peaks but not the primary peaks.

TABLE OF CONTENTS

LIST OF TABLES. v

LIST OF FIGURES vi

1.0 INTRODUCTION. 1

1.1 Introduction to Carbon Fiber Composites. 3

1.2 Thermoplastic vs. Thermosetting Resins 3

1.3 Introduction to PEEK and PPS 4

1.4 Poly(aryl-ether-ether-ketone) PEEK 5

1.5 Poly(phenylene sulfide) PPS. 6

1.6 Literature Review - PEEK 7

1.7 Literature Review - PPS. 11

1.8 General Theory of Crystallization in Polymers. . . . 12

1.9 Melting Temperature of Thin Polymer Crystals 20

1.10 Introduction to DSC. 24

2.0 EXPERIMENTAL. 29

2.1 The Perkin-Elmer DSC-2 29

2.2 Materials and Sample Preparation 32

2.3 Isothermal Crystallization of PPS. 34

2.4 Isothermal Crystallization of PEEK 37

2.5 T_m^* vs. T_c Analysis of PEEK. 38

2.6 PEEK - T_m^* vs. T_c (partial conversion) 40

2.7 T_m^* vs. T_c Analysis of PPS 41

2.8 PPS - T_m^* vs. T_c (partial conversion). 41

2.9 Microscopy 42

3.0 RESULTS 43

3.1 Isothermal Crystallization of PPS. 43

3.2 Isothermal Crystallization of PEEK 48

3.3 Crystallization Kinetics 51

3.4 Crystallization Kinetics - PPS 59

3.5 Crystallization Kinetics of PPS - Early Stages . . . 63

3.6 Crystallization Kinetics - PEEK. 64

3.7 T_m* vs. T_c Analysis of PEEK. 67

3.8 PEEK - T_m* vs. T_c (partial conversion) 74

3.9 Tm* vs. T_c Analysis of PPS 76

3.10 PPS - T_m* vs. T_c (partial conversion). 81

3.11 Microscopy 84

4.0 DISCUSSION. 88

4.1 Isothermal Crystallization Rates. 88

4.2 Crystallization Kinetics - PPS. 90

4.3 Crystallization Kinetics - PEEK 91

4.4 T_m* vs. T_c Analyses 96

5.0 BIBLIOGRAPHY. 102

6.0 APPENDIX. 105

A. PPS - Isothermal Crystallization Experiments 106

B. PEEK - Isothermal Crystallization Experiments. 109

LIST OF TABLES

Table		Page
I.	PPS - Isothermal Peak Positions.	44
II.	PPS/Fiber Film	44
III.	PEEK - Isothermal Peak Positions	49
IV.	PPS - Avrami Expoents.	61
V.	PEEK - Avrami Exponents.	65
VI.	PEEK - T_m^* vs. T_c.	70
VII.	PPS - T_m^* vs. T_c	79

LIST OF FIGURES

Figure		Page
1	. . . . .	22
2	PPS - Isothermal Peak Positions	45
3	PEEK - Isothermal Peak Positions.	50
4a	Isothermal Crystallization - PPS Composite, Phillips.	53
4b	Avrami Plot - PPS Composite, Phillips	54
5a	Isothermal Crystallization - PPS Composite, NASA. . .	55
5b	Avrami Plot - PPS Composite, Phillips	56
6a	Isothermal Crystallization, Neat PEEK	57
6b	Avrami Plot - Neat PEEK	58
7	PPS - Avrami Expoents	60
8	PEEK - Avrami Exponents	66
9	Neat PEEK - Melting Thermograms	68
10	PEEK APC-2 - Melting Thermograms.	69
11	PEEK - T_m* vs. T_c	72
12	Neat PEEK, APC-2 - Melting Thermograms.	73
13	Melting of Partially and Fully Crystallized PEEK. . .	75
14	Neat PPS - Melting Thermograms.	77

LIST OF FIGURES (cont'd)

15 PPS Composite - Melting Thermograms 78

16 PPS - T_m* vs. T_c. 80

17 Neat PPS, PPS Composite - Melting Thermograms 82

18 Melting of Partially and Fully Crystallized PPS . . . 83

19 Photomicrograph of Carbon Fibers in PEEK Film 85

20 Photomicrograph of Carbon Fibers in PPS Film. 87

21 Schematic of a Protospherulite. 93

1.0 INTRODUCTION

The two high temperature thermoplastics of interest in the study are poly(aryl-ether-ether-ketone) (PEEK) and poly(phenylene sulfide) (PPS). PEEK molding grade resin and PPS can crystallize to an extent of about 40% and 65% respectively. A polymer's thermal and mechanical properties, such as toughness, resistance to creep, glass transition temperature (T_g) and crystalline melting temperature (T_m) are critical to its use in composites. Such properties can be affected by degree of crystallinity and other crystalline characteristics such as crystallite size and perfection. Therefore, to optimize the properties of these resins to suit intended applications, one must understand their crystallizations and to control the resulting crystallinities.

The crystallizations of neat PPS and PEEK were the topics of several previous studies. However, their crystallizations in the presence of carbon fibers have not been studied much.

This study focuses on the ways carbon fibers influence changes in the crystallization kinetics of PEEK and PPS. Any effects of carbon fibers on the bulk crystallization of a polymer must involve the fiber/matrix interface. If the fiber/matrix interface can affect crystallization, it may also be that crystallization can affect the fiber-matrix interface. Effects on the interface can have significant consequences on

mechanical properties, since the most common modes of failure in fiber reinforced composites involve breakage at the fiber-matrix interface.

For the most part, this study involved thermal analysis experiments conducted via differential scanning calorimetry (DSC); supplemental experiments were conducted through the use of optical microscopy. Isothermal crystallization experiments and heating experiments were performed on the neat PPS and PEEK samples as well as on carbon fiber reinforced composite samples. Analysis of the crystallization isotherms obtained were performed using partial areas software developed by the Perkin Elmer Company. From the partial area analysis, crystallization kinetics parameters were determined. The heating analysis was used to determine the melting behavior of isothermally crystallized samples. An estimate of crystallite size and perfection was obtained from the analysis of the melting behavior. Optical microscopy was used to search for molecular orientation in the polymers caused by the presence of carbon fibers. The crystallization of both neat and carbon fiber containing polymers was observed with the use of a polarizing microscope equipped with a Mettler FP-2 Hot Stage.

1.1 Introduction to carbon fiber reinforced composites

Carbon fiber reinforced composites combine carbon fiber's high moduli and strength with the matrix polymer's high toughness and ductility. High moduli reduce fatigue and are desired for strain limited designs. But, even under low strains, high moduli materials tend to concentrate stresses and suffer brittle failure. Ductile materials will yield so as to redistribute the load, where brittle materials will fracture. The purpose of carbon fiber/polymer composites is to take the brittle carbon fiber and give it some pseudoductility to minimize local stress concentration [1].

1.2 Thermoplastic vs. Thermosetting Resins

Currently, thermosetting resins (thermosets) are the most commonly used matrix material in carbon fiber reinforced composites. The chemically reactive nature of thermosetting prepolymers that are used in the fabrication of composite products limits their shelf life and requires their storage under refrigeration. The lay-up and molding of thermoset composites can be done only once; the chemical cross-linking in thermosets is irreversible. Therefore, if a component is flawed, no reprocessing is possible. In addition, the repair or

combining of thermosets requires gluing, riveting, or some other means of superficial attachment.

High temperature crystallizable thermoplastic polymers (thermoplastics) have been eliciting increasing interest for use as matrix materials in carbon fiber reinforced composites. Thermoplastics offer many potential advantages over the thermosets in wide use today. Thermoplastics are usually polymerized to completion prior to composite fabrication and have and indefinite shelf life. Unlike thermosets, thermoplastics may be remelted and solidified many times. This allows components to be constructed in a series of successive remeltings. Damage in thermoplastics can also be repaired through remelting.

Thermoplastics have been criticized in that their lack of cross-links may allow them to creep. However, the lack cross-links also makes them less susceptible to brittle failure, and improves their toughness.

1.3 Introduction to PEEK and PPS

The tough, high melting, thermoplastics of interest in this study are poly(aryl-ether-ether-ketone)(PEEK) and poly(phenylene sulfide) (PPS). PEEK is a crystallizable aromatic polymer in which recurring benzene rings are para-substituted by a repeating sequence of two ether links followed by a carbonyl

link. PPS is a crystalline aromatic polymer in which recurring benzene rings are para-substituted with sulfur atom links.

PEEK

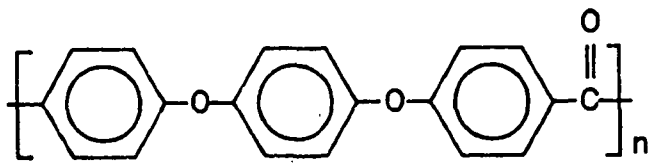

PPS

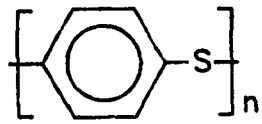

1.4 Poly(aryl-ether-ether-ketone) (PEEK)

Poly(aryl-ether-ether-ketone) (PEEK) was developed by Imperial Chemical Industries (ICI) and is marketed under the trademark VICTREX. A chemically correct name for PEEK is poly(oxy-1,4-phenyleneoxy-1,4-phenylenecarbonyl-1,4-phenylene).

PEEK can be synthesized by a nucleophilic aromatic substitution reaction, using diphenyl sulfone as a solvent, at temperatures near the melting point of the polymer [2,3,4]. Use of poly(phosphoric acid) and liquid HF as solvents for polymerization has also been reported.

The physical and mechanical properties of PEEK make it well suited for use as a matrix material in fiber reinforced structural composites. PEEK is tough. It exhibits ductile failure and also has high resistance to dynamic fatigue. It has good thermal stability and may be melted and crystallized

several times without significant chemical cross-linking or degradation. The polymer is highly insoluble. With the exception of some strong acids, no solvent has been found that readily dissolves it at room temperature [4]. PEEK is crystallizable. The maximum achievable degree of crystallinity is approximately 48% but typical values are usually around 30% [5]. The crystalline melting point is around 335 ^{o}C (608 K), and the glass transition temperature is around 145 ^{o}C (418 K) for the amorphous polymer and tends to be higher when crystallinity is present [6,7].

1.5 Poly(phenylene sulfide) (PPS)

Poly(phenylene sulfide) (PPS) is marketed by Phillips Chemical Co. under the trademark RYTON. The uncluttered aromatic ring and simple sulfur to carbon bond are highly stable. Its linear compact symmetrical structure causes PPS to be highly crystallizable; degrees of crystallinity may exceed 60 percent. T_m and T_g have been found to be 315^{o}C (588 K) and 92 ^{o}C (365 K) respectively [8]. Its resistance to a broad range of chemicals that is second only to polytetrafluorethylene (Teflon (R)). It is essentially insoluble; no substance has been found to dissolve PPS readily below 400 ^{o}F (570 K) [9].

Low molecular weight PPS is made by reacting

p-dichlorobenzene with sodium sulfide in a polar solvent. Higher molecular weight PPS suitable for injection molding is produced by heating the low molecular weight material in the presence of air. This process extends the chain length while producing some cross-linking.

In a new process, high molecular weight PPS is produced in one step by reacting p-dichlorobenzene with a small amount of an undisclosed comonomer in the presence of a catalyst. The resulting material is more linear and is of higher molecular weight, thus giving it higher strength and ductility than the PPS produced from from the conventional two step method [10].

1.6 Literature Review - PEEK

The following is a review of previous neat PEEK crystallization studies:

D.J. Blundell and B.N. Osborn conducted a study of PEEK crystalline morphology by DSC and X-ray diffraction. From plots of crystallization times vs. isothermal crystallization temperatures (T_c), they determined that the maximum rate of crystallization for PEEK occurs around 230 ^{o}C (503 K). By plotting crystallite lamellae thickness against T_c they obtained an extrapolated melting point (T_m) of 395 ^{o}C (668 K) which is the theoretical melting point of an ideal, infinitely large crystal. The heat of fusion for fully crystalline PEEK was determined to

be 130kJ/kg (31.07 cal/g) [11].

P. Cebe and S.-D. Hong used DSC to study the crystallization PEEK under isothermal and non-isothermal conditions. The Avrami exponent of crystallization time dependency [sec. 1.8] was found to be 3 from isothermal crystallizations. Non-isothermal crystallizations were analyzed by applying the Avrami equation at low conversion levels. Crystallization activation energies were calculated to be 68 kcal/mol. when cooling from the melt and 52 kcal/mol. when heating amorphous PEEK above Tg [12].

S.Z.D. Cheng, M.-Y.Cao, and B. Wunderlich studied the glass transition and melting behavior of PEEK via DSC. T_g was found to vary with crystallization temperature with lower crystallization temperatures giving higher T_g values. From isothermal crystallizations, three different populations of crystallites were identified: a high melting population which usually constituted a major portion of the crystallinity; a low melting population; and a broad but small fraction which crystallizes upon cooling the sample from T_c. Analysis of samples isothermally crystallized for different lengths of time indicated that the high melting crystals grow first followed by the low melting fraction. Effects of crystallinity on heat capacity (C_p) was also studied, and a rigid-amorphous fraction was identified in poorly crystallized samples which is non-crystalline yet does not contribute to the increase of C_p at T_g [7].

A. J. Lovinger and D. D. Davis crystallized PEEK from dilute solutions at temperatures near 210 ^{o}C (483 K) using two organic solvents (α-chloronaphthalene and benzophenone). Spherulites and single crystals were obtained. Crystalline morphology was studied with electron microscopy and diffraction. The crystallites were found to be fibrillar, being narrow in the a crystallographic axis and long in the b axis. The radial growth direction of the spherulites corresponded to the b crystallographic axis [13].

The following is a review of crystallization studies of PEEK in the presence of carbon fiber:

Y. Lee and R. Porter studied the crystallization of PEEK in the presence of carbon fibers using DSC and optical microscopy. Upon cooling from the melt, it was found that the presence of carbon fibers reduces supercooling required before PEEK crystallized, thus suggesting that the fibers act as nucleating agents. Fiber containing films were held in the melt at 390 ^{o}C (663 K) for prolonged periods and then crystallized by slow cooling. Photomicrographs obtained through the polarizing microscope show transcrystalline growth from the fiber surface and reduction of nucleation density in the bulk in samples that were held in the melt for two or more hours. Mechanical tests showed increases in transverse tensile strength and matrix/fiber adhesion for these samples [14].

F. N. Cogswell examined the crystalline texture of APC-1 PEEK/carbon fiber composites using optical microscopy. Nucleation of spherulites at the carbon fiber surface was noted for crystallization at 325 ^{o}C (598 K). Electron micrographs of broken composite sections show a PEEK polymer coating on the broken fiber ends, indicating high polymer to fiber adhesion [15].

D. J. Blundell, J. M. Chambers, M .W. Mackenzie, and W .F. Gaskin assessed crystallinity of PEEK matrix polymer in APC-2 carbon fiber composite with regard to degree of crystallinity and crystal orientation using X-ray diffraction and infrared reflection. The degree of crystallinity ranged from 20 to 40% with the higher values obtained at higher crystallization temperatures. In samples slowly cooled from the melt, an overall crystalline orientation bias was found with respect to the carbon fibers in which the crystallographic a-axis of PEEK was oriented perpendicular to the fiber axis [16].

1.7 Literature Review - PPS

The following is a review of studies of crystallization on neat PPS:

A. J. Lovinger and D. D. Davis used PPS to study regime II-III transitions by measuring spherulite growth rates at various crystallization temperatures under the microscope. In addition, DSC analyses were conducted to generate plots of melting points of a polymer that was isothermally crystallized at various T_c values, T_m* vs. T_c, from which an extrapolated crystalline melting point of 315 ^{o}C (588 K) was found for medium molecular weight PPS [8].

D.G.Brady conducted X-ray studies of PPS and determined the approximate degree of crystallinity in virgin grade (low molecular wt.) PPS to be 65 percent. In addition, tensile strength was found to decrease after annealing for low molecular weight PPS and increase in high molecular weight PPS [17].

F.J. Padden and A.J. Lovinger crystallized PPS from dilute solutions at temperatures 130-160 ^{o}C (403-423 K). The solvents used were α-chloronaphthalene and a mixture of α-chloronaphthalene and n-tetradecane. PPS films were also isothermally crystallized at temperatures up to 280 ^{o}C (553 K).

Examination under a scanning electron microscope revealed that spherulites were composed of extremely fine fibrils (as in PEEK) [18].

1.8 General Theory of Crystallization in Polymers

The crystallization process can be divided into two parts, nucleation and growth. Two types of nucleation will be considered; homogeneous nucleation in which nuclei form from the crystallizing polymer alone, and heterogeneous nucleation in which crystallization begins on foreign particles or on some other type of low energy site. (For the purposes of this discussion these low energy surfaces will be called impurities.) In crystalline growth, which occurs after nucleation, growth morphology and time dimensionality will be considered.

Nucleation is the mechanism by which crystallites are formed and grown to a stable size. Below the melting point of the polymer a bulk crystalline phase will be thermodynamically more stable than a molten phase, but the initiation of crystallite formation is often accompanied by a rise in free energy which thus acts as a barrier to crystallization. This barrier is caused by the high surface area to volume ratios that are characteristic of small crystallites in comparison to large ones. The surface free energy associated with these small crystallites, which opposes crystallization, will outweigh their

heat of fusion thus causing instability. Crystallites which reach a critical size may continue to spontaneously grow to stable crystals. Critical size may be defined as the size at which any additional growth lowers the free energy barrier to phase transition. A critical size arises because the volume of the new phase grows in proportion to the cube of its increase in linear dimensions while its surface grows proportionally to the square of those dimensions.

Two mutually exclusive categories of nucleation are termed homogeneous and heterogeneous. In homogeneous nucleation, polymer segments are brought together through random thermal motion, forming nuclei of various sizes. Small nuclei are unstable and will remelt. Nuclei of critical size will continue growing and will become thermally stable.

In heterogeneous nucleation, nucleation occurs on the surfaces of impurities. The impurity lowers the free energy barrier to nucleation by contributing to a surface energy more favorable to crystallization than does the melt. Also, the impurity may contain cracks or channels that can prealign polymer segments for crystallization. In the ideal case, the heterogeneities totally eliminate the free energy barrier to nucleation; all nucleation will occur the instant the polymer is lowered below its melting point.

Crystalline Growth

After nucleation has occurred, the resulting crystallite will continue to grow, incorporating material from the melt. As growth proceeds, the crystallizing mass will attain a specific growth morphology, which changes in a continuous manner, outwardly from the point of nucleation. For common growth morphologies, the total amount of material converted to the crystalline phase as a function of time may be given by:

$$\text{conversion} = kt^n \qquad (1.1)$$

The time exponent n is known as the Avrami exponent named after M. Avrami, who developed a general theory of phase growth [19,20]. The Avrami exponent is the time dimensionality of crystalline phase growth. It is a summation of the crystalline growth dimensionality and the time order of nucleation. Spherulitic growth will be used as an example, since it is the most common growth morphology observed in crystallizable polymers.

Spherulitic crystalline growth from randomly forming nuclei (homogeneous nucleation) is characterized by an Avrami exponent of 4. The volume increase of a sphere will be a cubic function of its radius increase. Therefore, assuming linear growth rate to be constant, the volume increase of a sphere will be a cubic

function of time. With constant nucleation rate, the number of spheres formed will be a first-order function of time. The rate of initiation of spheres multiplied by the growth rate of individual spheres will give the overall rate of amorphous to crystalline transformation. In this case it will be fourth-order with respect to time.

If nucleation is ideally heterogeneous, the number of nuclei will not be a function of time. The number of nuclei formed will be predetermined by the number of heterogeneities present and will all form simultaneously at the beginning of the crystallization. In this case, the dimensionality of the growth process alone will contribute to the Avrami exponent. Spherulitic growth from ideal heterogeneous nucleation will generate an Avrami exponent of three.

Derivation of growth kinetics for spherulitic growth from homogeneous nucleation will be given as an example. Two cases will be considered. The first will use the so-called free growth approximation in which nucleation and growth of spherulites are considered to be independent of other spherulites present. In the second case, limitations on nucleation and growth of spherulites by the presence of other spherulites will be considered.

Spherulitic Growth Kinetics - Free Growth Approximation

When nucleation is a random process (homogeneous case) the number of nuclei to form in the time period t may be given by:

$$n = NM_o t \quad \text{or} \quad dn = NM_o dt \tag{1.2}$$

where n is the number of nuclei, and M_o is the total mass of the crystallizing material, and N is the nucleation rate with dimensions $[n.mass^{-1}.time^{-1}]$.

If linear growth rate is constant, then the radius of a spherulite at any time t will be given by:

$$r = G(t - t_i) \tag{1.3}$$

where G is growth rate in units of distance/time, and t_i is the time at which the spherulite was nucleated.

The differential change in crystalline mass (dM_c) may be given by:

$$dM_c = N(M_o)dt_i(4/3)\pi G^3(t - t_i)^3\rho_c \tag{1.4}$$

ρ_c is the density of the crystalline phase.

Total crystalline mass M_c at time t is obtained by integration

of (1.4) between the limits of $t_i = 0$, and $t_i = t$ which yields

$$M_c = M_o[(\pi/3)N(G^3)(\rho_c)]t^4 \qquad (1.5)$$

Dividing by M_o and making the constants in the brackets one constant gives:

$$M_c/M_o = [k]t^4 \qquad (1.6)$$

Spherulitic Growth Kinetics with Impingement

Equation (1.6) holds only when M_c is very small in relation to M_o. As M_c gets larger, spherulites will impinge. In addition, the remaining uncrystallized mass will be reduced, thereby reducing the rate of new nucleation. The rate of change in crystalline mass with impingements considered may be related to the change in crystalline mass growing freely by the following equation:

$$dM_c(\text{impinged})/dM_c(\text{free}) = 1 - M_c/M_o \qquad (1.7)$$

$dM_c(\text{free})$ is obtained by differentiation of equation (1.5) with respect to time:

$$dM_c(\text{free}) = M_o[(4\pi/3)N\ G^3\ \rho_c]t^3dt \qquad (1.8)$$

Substitution of equation (1.8) into (1.7) gives:

$$dM_c(\text{impinged})/(M_o - M_c) = [(4\pi/3)NG^3\rho_c]t^3dt \qquad (1.9)$$

Integration of (1.9) gives:

$$-\ln(1 - M_c/M_o) = [(\pi/3)NG^3\rho_c]t^4 \qquad (1.10)$$

Combining the terms in the brackets and expressing (1.10) as an exponential gives:

$$1 - M_c/M_o = \exp(-kt^4) \qquad (1.11)$$

Implicit in equation (1.11) is that crystallization goes to completion. That is to say, given enough time, the sample will become totally crystalline. Polymeric materials seldom, if ever, crystallize entirely. The PEEK and PPS samples, which are the subject of this report, typically crystallize to between 30 and 65% of the total sample mass. The above analysis must be

modified to accommodate materials which never crystallize to completion. Equation (1.6) can be rewritten as:

$$dM_c(\text{impinged})/dM_c(\text{free}) = 1 - M_c/M_o(M_o/M_{c,\infty}) \qquad (1.12)$$

The presence of M_c places some of the remaining amorphous material in an uncrystallizable situation. The term $(M_o/M_{c,\infty})$ is a correction factor to account for the total sample fraction that becomes uncrystallizable with M_c.

Replacing equation (1.7) with equation (1.12) and integrating as was done with equation (1.9) yields:

$$-\ln [1 - X_c(t)/X_c(\infty)] = 1/X_c(\infty)kt^n \qquad (1.13)$$

where $X_c(t)$ and $X_c(\infty)$ equal the mass fraction of crystallinity after time t and the mass fraction of crystallinity at infinite time.

The time dependency of conversion during isothermal crystallization can be analyzed using equation (12)

$$X_c(t)/X_c(\infty) = 1 - \exp(-k't^n) \qquad (1.14)$$

where $k' = [1/X_c(\infty)]k$.

1.9 Melting Temperatures of Thin Polymer Crystals

For the purposes of evaluating melting point data later in this report, it will be useful to describe the factors influencing the observed melting temperatures of polymer crystallites.

The theoretical equilibrium melting temperature of a polymer crystal T_m may be defined as the temperature at which a polymer crystal of infinite size and complete perfection will melt. The actual melting temperatures observed in crystallizable polymer systems T_m^* are usually found well below T_m. Polymer crystals tend to be small and imperfect with thicknesses related to crystallization temperature T_c. The creation of large surface areas associated with the formation of small crystals adds a significant surface energy quantity to the free energy of formation thereby lowering melting temperature.

Polymers tend to crystallize into flat lamellae which are thin in the chain direction with upper and lower surfaces consisting mostly of chain folds (Fig. 1). Spherulites, if allowed to grow in an unrestricted way, are aggregates of lamellae stacked either parallel or perpendicular to the radial direction. Lamella thickness is the predominant factor determining melting point depression, and crystallization temperature is the predominant factor determining lamella thickness.

J.D. Hoffman and J.J. Weeks [21] and L. Mandelkern [22] have derived expressions relating T_m^* to lamella thickness, and relating lamella thickness to T_c. Thereby, expressions are derived relating T_m^* to T_c. The following is an extract from those derivations.

The free energy of formation of the crystal in Fig. 1 is given by:

$$\Phi_c = 2ab\sigma_e + 2b\underline{l}\sigma + 2a\underline{l}\sigma - ab(\Delta f) \qquad (1.15)$$

σ_e is the surface energy of the (a x b) face possessing the chain folds. σ is the surface energy of the (a x $\underline{l}$) and (b x $\underline{l}$) faces.

Δf is the free energy difference between the crystalline phase and the liquid phase. f may be approximated as follows:

$$\Delta f = (\Delta H_f)(T_m - T_m^*)/T_m \qquad (1.16)$$

This approximation is somewhat crude in that it assumes that the entropy change associated with the phase transition at Tm* equals $\Delta H_f/T_m$, but its present form is accurate enough for this discussion.

At T_m^*, Φ_c will equal zero. Inserting equation (1.16) into (1.15) gives:

$$T_m^* = T_m[1 - 2\sigma_e/(\Delta H_f)l] \qquad (1.17)$$

terms including do not appear in equation (1.17) because the crystal in Fig.1 is assumed to be very large in the a and b dimension thereby making insignificant surface energy contributions from the (a x $\underline{l}$) and (b x $\underline{l}$) faces.

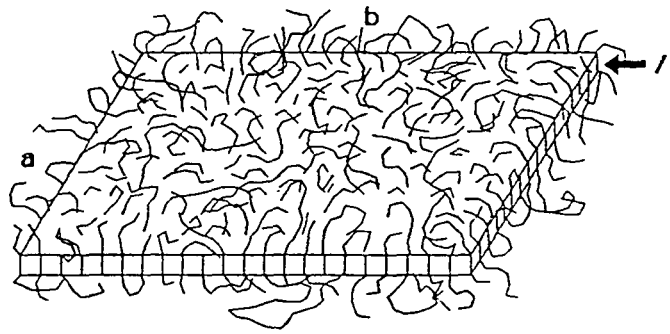

Fig.1

The relationship between lamella thickness and T_c is not as straightforward as that between lamella thickness and T_m. In the formation of the crystalline lamella, the thickness of crystal growth will mimic the thickness of the primary growth nucleus. Polymer chains adhering to a growing crystal face will tend to fold regularly at the face edge. Growth from chains folding above the existing face edge will be inhibited by the energy required to create the additional crystal surface in contact with the melt. Growth from chains folding below the existing face edge will be inhibited by the

energy required to create an additional edge plus the instability associated with a thinner crystallite.

The thickness of the primary growth nucleus is dependent on T_c. The thickness $\underline{l}^*$ of the primary, bundle-like growth nucleus in the chain direction for an infinitely long chain is given by:

$$\underline{l}^* = 4\sigma_e/\Delta f = 4\sigma_e T_m/[\Delta H_f(T_m - T_c)] \qquad (1.18)$$

If crystalline growth from the primary nucleus consists mostly of chain folding with $\underline{l}$ remaining approximately equal to $\underline{l}^*$, and if σ_e of the crystal equals σ_e of the nucleus, then equation (1.18) may be substituted for $\underline{l}$ in (1.17) giving:

$$T_m^* = 1/2(T_m + T_c) \qquad (1.19)$$

More generally, $\underline{l}$ is not necessarily equal to $\underline{l}^*$ but is proportional to $\underline{l}^*$ by $\underline{l} = \beta\underline{l}^*$, and substitution of (1.18) into (1.17) gives:

$$T_m^* = T_m[1 - 1/(2\beta)] + T_c/(2\beta) \qquad (1.20)$$

β must be at least 0.5 to satisfy requirements for thermal stability.

Plotting T_m^* vs. T_c should give a straight line with a slope of

$1/(2\beta)$. T_m can be obtained by extrapolating the plot to $T_m^* = T_c$.

In the case where nucleation is a homogeneous two-dimensional process such as in the deposition of a monolayer of polymer chains on the face of an existing crystallite

$$\underline{l}^* = 2\sigma_e / f = 2\sigma_e T_m / [\Delta H_f (T_m - T_c] \quad (1.21)$$

for an infinitely long chain. Then, as shown above for the bundle-like nucleus,

$$T_m^* = T_m(1 - 1/\beta) + T_c/\beta \quad (1.22)$$

Here, a plot of T_m^* vs. T_c would yield a straight line with a slope of $1/\beta$. For the special case in which $\underline{l} = \underline{l}^*$, the slope would be 1.0.

1.10 Introduction to DSC

Experimental results presented in this report were obtained primarily by DSC. Put simply, a DSC measures the rate at which heat travels to or from a sample while the temperature of that sample is either held constant or changed at a predetermined rate. Through these heat flow measurements, enthalpies associated with first order transitions and changes in heat capacity associated with second order transitions can be

calculated. In this report, DSC was used to measure the heats of crystallization and melting with focus on the rates and temperatures at which these transitions occurred.

A DSC sample chamber has identical sample and reference holders. Both holders are in contact with a sub-ambient, constant temperature source but are insulated from each other. Each holder is equipped with a platinum resistance thermometer and heating coil. When in operation, the two holders are maintained at equal temperatures at all times by a closed loop control of the electrical power provided to the heating coils. Energy per unit time which is absorbed or evolved by the sample must be exactly compensated by a corresponding increase or decrease of power sent to the sample holder relative to the reference holder. Measurement of the power difference between the sample and reference holders is recorded as energy flow to or from the sample. A curve is generated of energy flow vs. time, but is most commonly plotted as energy flow vs. temperature when temperature changes at a fixed rate. If heat generated by the sample per unit time, dh/dt, is designated as being negative and heat absorbed by the sample as positive, then, for the case where temperature changes at a fixed rate, a basic equation relating dh/dt to instrumental quantities can be given as [23]:

$$dh/dt = dq/dt - (C_s - C_r)dT_p/dt + RC_s(d^2q/dt^2) \qquad (1.23)$$

dq/dt is the heat flow rate to the sample from the heat source, T_p is the temperature of the heat source, dT_p/dt is the programmed heating rate, C_s is the heat capacity of sample plus the sample holder, C_r is the total heat capacity of the reference holder, and R is the thermal resistance of the path dq/dt must travel to and from the sample.

Accuracy of thermal measurements is improved when the second term in equation (1.21) is kept as close to zero as possible by matching the heat capacities of the sample and reference holders. To accomplish this, an empty sample pan weighted with extra pan covers in order to approximate the heat capacity of the sample, was placed in the reference holder.

The third term in equation (1.21) represents a thermal lag which requires consideration when determining melting peak positions and temperature calibration.

During sharp transitions, such as the melting of metal standards, C_s in equation (1.21) goes to infinity and the equation may be rewritten as [24]:

$$d^2q/dt^2 = (1/R)(dT_p/dt) \qquad (1.24)$$

Here, the slope of the energy flow curve will not be infinite, as

a sharp transition would dictate, but will be of some finite maximum value as a result of the thermal resistance and heating rate. (d^2q/dt^2 is the slope of the energy flow curve). For this reason, when reading the melting temperatures of sharp transitions, it is necessary to designate the onset of the melting peak as the true melting point and not the peak maximum. In this study, only the metal standards used for temperature calibration had melting temperatures that were so narrow as to require this consideration. The melting temperatures of the polymers analyzed in this study were broad; spanning tens of degrees. For such wide melting bands, it is appropriate to designate the melting peak maximum, which is indicative of the most populous crystalline species, as the melting temperature.

Heating rate introduces a thermal lag correction to temperature calibration arising from the heat capacity of the sample holder. The temperature difference between the sample temperature and heat source temperature with respect to heating rate may be given as [24]:

$$T_p - T_s = RC_s(dT_p/dt) \qquad (1.25)$$

The correction is made by melting a standard at various heating rates to determine RC_s. RC_s may be assumed to be constant because the heat capacity of the sample holder is much larger

than that of the sample (sample masses used were on the order of 10 mg).

2.0 EXPERIMENTAL

2.1 The Perkin-Elmer DSC-2

The DSC used in this study was a Perkin-Elmer model DSC-2. The basic instrument consists of a sample head with its supporting electronics. An accessory refrigeration unit which provides a sub-ambient constant temperature source is connected to the sample head. The sample head is enclosed in a glove box and is flushed with nitrogen to prevent the formation of frost. The instrument panel contains controls for setting heating and cooling rates and temperature limits. Controls for baseline adjustments, temperature calibration, and energy calibration are also available. Thermal data generated by the DSC is transmitted to a Perkin-Elmer model 3600 data station.

The Perkin-Elmer 3600 data station is similar to a personal computer. It has two floppy disk drives. One drive runs Perkin-Elmer thermal analysis software. The software can process raw data from the DSC and can analyze data after being stored. On a disk in the other drive data is stored that may be retrieved for future analysis or plotting.

In this study, two software programs were used. One was TADS (Thermal Analysis Data Station), which is used when measurements of heat flow are taken while temperature is changing at a fixed

rate. The other was isothermal software, which is used when measurements of heat flow are taken while temperature remains constant.

The TADS software was used to set up and run heating analyses and to process raw data from the DSC. During a scan, incoming data is displayed on a CRT both numerically and graphically. In the latter case, energy flow in mcal/sec is displayed on the ordinate and temperature in Kelvin is displayed on the abscissa. After completion of a heating scan, the TADS software was used to analyze the thermometric data curve with respect to positions of peak maxima and peak area. Peak areas, determined by the TADS software, are divided by scan rate and sample mass, thus yielding heats of transition of the sample expressed in cal/g.

The isothermal software operates essentially in the same manner as the TADS software except that data is displayed as energy flow vs. time instead of temperature. With the isothermal software, partial peak areas as well as total peak area can be measured in order to calculate the fraction of a transition completed at any time.

A lead metal standard, provided by Perkin-Elmer, was melted in the DSC at 20, 40, 80, and 160 K/min and the apparent melting temperatures were recorded. Thermal lag with respect to heating rate was calculated using equation (1.23) as outlined in sec.

1.10. RC_s was determined to be 0.116 sec. The procedure was repeated to assure accuracy. (To enhance readability, isothermal temperatures listed in the following sections of this report have not been corrected with respect to heating rate unless otherwise indicated. Absolute temperature calibration of the DSC was carried out using a heating rate of 20 K/min, therefore, 2.3 K must be added to the listed isothermal temperatures to obtain absolute temperatures.)

Prior to each DSC experimental session, the temperature calibration of the instrument was carefully checked and adjusted. Thermal studies of PEEK and PPS polymers required the use of the DSC in a temperature range spanning 350 K to 680 K, therefore, lead (m.p. 600.65 K) and indium (m.p. 429.78 K) standards were chosen for calibration of both temperature range and zero. Each standard was melted at 20 deg/min, and the indicated melting temperature was recorded. The temperature range and the zero controls were adjusted until the indicated melting temperatures of the standards were within +/- 0.2 K of the actual melting temperatures. The temperature calibration was rechecked every two hours during the experiments to insure it remained within these limits. Thermal data obtained while temperature calibration was drifting out of limits was discarded.

2.2 Materials and Sample Preparation

Neat PPS resin (MR03, Sa# 58641) made by the Phillips Petroleum company was used as a control in this study. Two carbon fiber reinforced composite panels incorporating PPS MR03 resin were studied. The first panel, sample # GD441, was prepared at NASA-Langley Research Center. The second panel, sample # 58306, was prepared by Phillips Petroleum. In this study, most of the experiments were carried out on the former rather than the latter panel.

The neat PPS resin was obtained in powder form. To convert it into an amorphous fused mass, the powder was placed on Kapton film and melted in an oven at 615 K for two min in air and then quickly quenched in ice water. Of those tried, these time-temperature conditions were found to produce wholly amorphous PPS with the least discoloration. Areas of little or no discoloration were cut from the quenched samples and saved for DSC experiments.

As received, the PPS/carbon fiber composite samples studied were small pieces of uniaxial panels, approximately 0.2 cm thick. These were sawed into strips perpendicular to the fiber direction with a coping saw. From these strips, samples of the desired size could be easily sheared off with a razor blade. To render the PPS in the composites amorphous, composite samples were placed in a 615 K oven for 5 min and then quenched in ice

water.

Neat PEEK resin (ICI, Sa# 9211/43) made by Imperial Chemical Industries was used as a control in this study. Two carbon fiber reinforced composite materials incorporating PEEK resin, APC-1 and APC-2, were studied. APC is an ICI designation standing for Aromatic Polymer Composite [15]. APC-2 was introduced after APC-1 and is said to be more uniform and exhibit better mechanical properties than APC-1. Two APC-2 panels, sample # GD432 and sample # GD433, which were prepared at NASA-Langley research center, were the focus of most experiments in this study. An APC-1 panel, # 2/397, which was prepared by ICI, was examined mainly to reinforce comparisons made between APC-2 and the neat PEEK resin.

The neat PEEK resin was obtained in pellet form. To produce amorphous resin, pellets were placed between Kapton films in a heated press at 660 K for 4 min then quenched in ice water. This method produced clear transparent films of a uniform amber color which is characteristic of amorphous PEEK. Samples weighing around 10 mg were cut and placed in aluminum DSC sample pans.

PEEK/carbon fiber composite samples were cut in the same manner as were the PPS composites. Sample masses were from 20 to 30 mg. These samples had each been melted once and immediately cooled in a previous study [25]. To render the PEEK

in the composites amorphous, composite samples were placed in a 677 K oven for 5 min then quenched in ice water.

Samples were weighed and placed in aluminum DSC sample pans. The sample pans were crimped shut by hand with tweezers. It was found that crimping by this method left the bottom of the sample pans much flatter than if they were crimped with the crimping tool provided by Perkin-Elmer. This flatness is required for good thermal contact with the DSC head. The composite sample masses were between 20 and 30 mg and the neat resin samples weighed approximately 10 mg. Samples were prepared form both amorphous and partially crystalline materials.

2.3 Isothermal Crystallization of PPS

High and low temperature isothermal crystallizations of PPS resin and its composites were carried out in the DSC. Prior to each high temperature crystallization, the sample was cooled rapidly from the melt to some T_c below the melting temperature of a perfect crystal $T_{m,eq}$ but above the temperature of maximum crystallization rate T_{max}. For low temperature crystallizations, a sample quenched to the amorphous state was heated rapidly from below T_g to some T_c which is below T_{max}.

Data collection began when the sample reached T_c. The data as represented on the DSC computer, was expressed as energy flow in millicalories per second (mcal/s) vs. time in min.

All crystallization thermograms which were suitable for analysis of crystallization kinetics had certain characteristics in common (Fig. 2a, 3a and 4a). In the initial portion of the thermogram the energy flow curve would slope sharply as the sample head was achieving thermal equilibrium; then it would flatten out, establishing a horizontal baseline. As the sample would begin to crystallize, the the energy flow curve would dip down in response to energy being given off by the sample. The data plotted would go through a minimum corresponding to the maximum crystallization rate of the sample, then slowly rise and level off at the horizontal baseline as the crystallization ceased.

Due to instrumental limitations, most of the crystallization temperature range in the region between T_g and T_m was not accessible for study. At temperatures near T_{max}, crystallization would begin before thermal equilibrium could be established. At temperatures near T_g and T_m, crystallization was too slow to be accurately measured. Approximate temperature ranges where meaningful data could be collected were 480-510 K for the high temperature crystallizations and 385-405 K for the low temperature crystallizations.

To carry out a low temperature crystallization, the sample chamber's temperature was set at 350 K, which is approximately 11° below the T_g of PPS. A quenched amorphous sample was

loaded into the chamber and heated at 320 K/min to T_c. When thermal equilibrium was established, which typically took 0.5 min, the energy ordinate value was noted. As crystallization progressed to completion, the ordinate value would return to its equilibrium position, and data collection was terminated. Several crystallizations were carried out at different temperatures for both the neat resin and NASA carbon fiber composite. Many crystallizations were carried out at the same temperatures to evaluate reproducibility.

To carry out a high temperature crystallization, a sample was heated at 320 K/min to 600 K. It was held at that temperature for 1 min and then cooled at 320 K/min to T_c. Thermal equilibration typically took about 0.8 min to be established, and, as in low temperature crystallizations, data collection was terminated when the ordinate value returned to its equilibrium position. Several crystallizations were carried out at different temperatures for the neat resin, the NASA composite, and the Phillips composite. To see if initial melting in the 615 K oven affected crystallization kinetics, quenched amorphous samples used in the low temperature crystallizations were reused and compared to fresh samples. Most samples were remelted two additional times then compared to fresh samples to check thermal stability. In addition, two samples were heated to 600 K and held there for 5 min, instead of the usual 1 min, to check ther-

mal stability.

There was concern that differences noted in crystallization kinetics between the composite and neat polymer may be due to differences in resin formulations. To check this, a fiber-containing film was prepared from the neat resin used as the control in the above. Chopped graphite fibers (Hercules type AS-4) were mixed with neat PPS MR03 powder. The mixture was placed between two Kapton(R) films and placed in a 593 K press for 2 min then quenched in ice water. Regions where fibers were most abundant were cut out and saved for crystallization experiments. A second film, to be used as a control, was prepared in an identical manner but with the fibers omitted. Isothermal crystallizations of these samples were carried out at 490 K and 495 K.

2.4 Isothermal Crystallization of PEEK

Isothermal crystallizations of PEEK were carried out in much the same manner as those of PPS. Specific temperatures were higher to accommodate the higher melting temperatures of PEEK, but the experimental procedures were essentially the same. Sample preparation differed slightly in that neat PEEK amorphous samples were prepared using a heated press instead of the oven.

Temperature ranges in which meaningful data could be collected were approximately at 570-590 K for high temperature

crystallizations and 430-440 K for low temperature crystallizations. To carry out low temperature crystallizations, the DSC sample head was set at 400 K which is approximately 18° below the T_g of PEEK. A quenched amorphous sample was loaded into the into the head and heated at 320 K/min to T_c. To carry out high temperature crystallizations, the sample was heated at 320 K/min to 670 K. It was held at that temperature for 2 min then cooled at 320 K/min to T_c.

To insure that the samples heated to 670 K were being completely melted and purged of any thermally sensitive nucleation sites, two samples were heated to 680 K where they remained for 2 min. For comparison, they were then crystallized under the same conditions as samples heated to 670 K. Three samples which had been used in low temperature crystallizations were remelted and used in high temperature crystallizations. These were compared to fresh samples to see if melting in the 677 K oven had affected their crystallization kinetics. In addition, two samples were held in the 677 K oven for 12 min, instead of the usual 5 min, to check thermal stability.

2.5 T_m* vs. T_c Analysis of PEEK

T_m* vs. T_c analysis were carried out on PEEK before they were performed on PPS. Experiments were carried out on PEEK composites to insure thermal lag errors were not arising from

the large composite sample masses used in this study. It is, therefore, useful to list these experiments first.

In T_m* vs. T_c experiments, samples were melted in the DSC after isothermal crystallization therein. Their melting behaviors were recorded and correlated with the crystallization conditions.

The procedure used for neat PEEK and PEEK composite samples follows: Samples were heated to 670 K and held at that temperature for 2 min. They were then cooled at 320 K/min to T_c and held there for 10 min, unless additional time was required to complete the crystallization. Results from previous isothermal crystallization studies were used to determine when crystallization times would exceed 10 min. After isothermal crystallization was complete, the samples were cooled from T_c to 520 K at a rate of 320 K/min. A heating scan was taken from 520-K to 650 K at a heating rate of 40 K/min, and thermal data was collected.

Data obtained at seven crystallization temperatures were used at 10^{o} intervals from 530 K to 590 K. To check reproducibility and to assure that complete melting was being achieved, a sample was heated to 680 K instead of the usual 670 K prior to crystallization. The crystallization of this sample was carried out at 550 K. The results were then compared to a sample prepared at 670 K, also crystallized at 550 K.

The masses of the PEEK composite samples were two to three

times greater than the neat PEEK samples. (This was also true of the PPS samples.) There was concern that these differences in mass would give rise to unequal thermal conductivities between the two samples. Significant differences in thermal conductivities will cause apparent temperature shifts of thermal data. To be assured that significant differences in thermal conductivities were not important, a composite sample of similar weight to the neat samples was crystallized at 550 K and compared to the larger composite samples.

2.6 PEEK - T_m^* vs. T_c (partial conversion)

To study chronological order in which different crystalline species form, heating scans were taken of a neat PEEK sample that was first partially and then totally crystallized at 585 K. In the partial crystallization, the sample was cooled from 670 K to 585 K at 320 K/min and held at that temperature for 6.0 min, the approximate time required to reach the maximum crystallization rate. A heating scan was then immediately undertaken without any further cooling of the sample. The procedure for the completely crystallized sample was identical, except it was held at 585 K for 20 min instead of 6.0 min.

2.7 T_m^* vs. T_c Analysis of PPS

The procedure by which neat PPS and PPS composite samples were analyzed was much the same as in the PEEK study. However, different crystallization temperatures were required to accommodate the lower melting temperatures of PPS.

A typical sample was heated to 600 K and held at that temperature for 1 min. The sample was then cooled at 320 K/min to T_c. It remained at T_c for 10 min, unless additional time was required to complete the crystallization. As in PEEK studies, results from previous isothermal crystallization studies were used to determine when crystallization times would exceed 10 min. After isothermal crystallization was complete, the sample was cooled from T_c to 430 K at 320 K/min. A heating scan was taken from 430 K to 580 K at a heating rate of 40 K/min and thermal data was collected.

Seven crystallization temperatures at 10° intervals from 440 to 500 K were employed here. To check reproducibility, crystallization at 470 K was carried out on a fresh sample and on a sample that had been cycled three times. This was done for both PPS composite and and neat PPS samples.

2.8 PPS - T_m^* vs. T_c (partial conversion)

A study of the order in which different crystalline species form was carried out for PPS in a similar manner as was done for

PEEK. Heating scans were taken of a neat PPS sample that was first partially and then completely crystallized at 485 K. To carry out the partial crystallization, the sample was cooled from 600 K to 485 K at 320 K/min and held at that temperature for 2.75 min, the approximate time required to reach maximum crystallization rate. A heating scan was then immediately performed without any further cooling of the sample. The procedure for the completely crystallized sample was identical, except it was held at 485 K for 15 min instead of 2.75 min.

2.9 Microscopy

PEEK film containing carbon fibers was prepared in the heated press. Carbon fibers were thinly spread over a PEEK film and covered with a second PEEK film. The sandwich, placed between Kapton films, was put in a 660 K press for 4 min and then quenched in liquid nitrogen. The Kapton film was removed and the PEEK/fiber film was saved for later observation under a polarizing microscope.

PPS film containing carbon fibers was prepared in the same fashion as with PEEK with the exception that the PPS sample was held in the press at 593 K for 2 min and quenched in ice water.

3.0 RESULTS

3.1 Isothermal Crystallization of PPS

The total areas of exothermic peaks in crystallization thermograms were measured and peak minima were determined using the Perkin-Elmer 3600 data station.

The positions of the minima are equivalent to the time required for the sample to reach maximum crystallization rate (t_{max}). For purposes of the following discussion, crystallization rates will be considered inversely proportional to t_{max}. The time required to reach maximum crystallization rate at each temperature (isothermal peak positions) for the PPS composites and the PPS neat resin samples are listed in Table I. Plots of t_{max} vs. T_c are given in Fig. 2.

From Table I and Fig. 2, it can be seen that the carbon fiber composite samples crystallize much more rapidly than the neat PPS resin. At most crystallization temperatures, the composite samples crystallize two to three times more rapidly than the neat resin. The crystallization rates of the composite samples prepared by Phillips Petroleum were slightly lower than those found for the NASA composites, but these differences are small compared to the much slower crystallization rates of the neat resin.

Table I

PPS - Isothermal Peak Positions

T_c (K)	Neat PPS t_{max} (min)	NASA GD441 t_{max} (min)	Phillips 58306 t_{max} (min)
385	——	9.71, 9.60	——
390	8.76	3.72	——
395	4.08, 3.82	1.78	——
400	2.09	1.11	——
405	1.04, 1.16	——	——
475	1.62	——	——
480	1.79	——	——
485	2.87, 2.45	1.14	——
490	4.07, 4.41	1.49	1.90
495	6.84	1.86, 1.86	2.59
500	11.13	2.77, 2.69 2.21	3.86, 4.30
505	20.64	4.39, 3.80 4.50, 3.67	6.06
510	——	6.75, 7.48	——
515	——	11.4	——

Table II

PPS/Fiber Film - Isothermal Peak Positions

T_c (K)	Neat Film t_{max} (min)	Fiber Film t_{max} (min)
490	3.13, 3.12	2.64, 2.84
495	4.27, 4.45	3.68, 4.02

Fig. 2 PPS – ISOTHERMAL PEAK POSITIONS

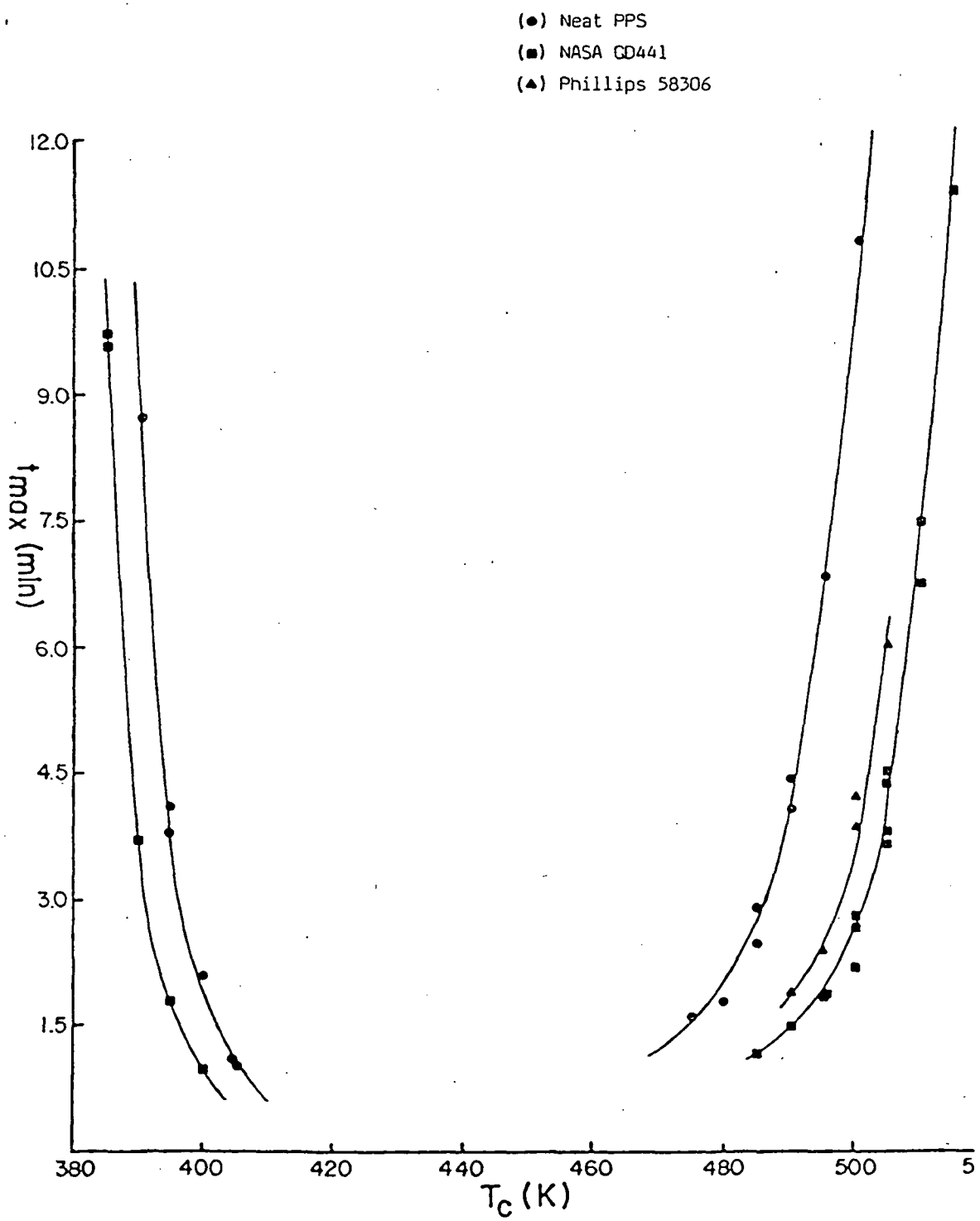

The curves of t_{max} vs. T_c for the composites and neat resin samples are of similar shape if translated along the temperature axis. In the high temperature region, the composite sample curve shows an approximately 15^{o} increase in displacement relative to the neat resin curve. Thus, the composite can crystallize as rapidly as the neat resin at a T_c of about 15^{o} higher than that of the neat resin. In the low temperature region, the difference is not as great; the composite sample curve is displaced approximately 5^{o} lower than the neat resin curve.

Differences in thermal history show little or no affect on the crystallization rates of either the PPS composite samples or the neat PPS resin samples. The thermal history of each sample before isothermal crystallization is given in the appendix. The number of cycles indicates the number of times the sample was held at 600 K for 1 min prior to that crystallization. The notation "Ov" indicates that the sample had been melted in an oven (see sec. 2.2, Materials and Sample Preparation). Samples which had been cycled a number of times appear to crystallize less rapidly. However, the effect appears to be small and perhaps insignificant. The two samples held at 600 K for 5 min before crystallization (#01215 and #01216) behaved no differently in this respect than the samples held at 600 K for the usual 1 min before crystallization.

Degrees of crystallinity attained in the isothermal crystallizations of the neat PPS samples are listed in the appendix. These values were calculated by dividing the thermogram peak area by an accepted heat of fusion values for a PPS crystal (23.9 cal/g [26]). Degrees of crystallinity attained in the isothermal crystallizations of the PPS composite samples were not calculable since fiber content was not known. Attempts to determine the fiber content of these samples, by density measurement, were frustrated by the apparent presence of voids.

The PPS MR03 film containing chopped carbon fibers crystallized more rapidly than a similar film in which the carbon fibers were omitted. Times to maximum crystallization rate are listed in Table II.

The neat PPS film used as the control in the above experiment, was prepared in the 593 K press. This film crystallized more rapidly than either the neat PPS samples melted in the 615 K oven, or those used in the powder form. This may be due to the occurrence of biaxial orientation during processing for samples prepared in the heated press.

3.2 Isothermal crystallization of PEEK

Isothermal crystallizations of PEEK were analyzed in the same manner as were those for PPS. Times to maximum crystallization rate (t_{max}) at various temperatures for the PEEK composites and neat PEEK resin samples are listed in Table III. Plots of t_{max} vs. T_c are given in Fig. 3.

As was the case with PPS, the PEEK composite samples also crystallized much more rapidly than the neat PEEK. The difference is not as great as noted in the PPS system, yet this difference is definitive and reproducible. Again, the curves of t_{max} vs. T_c for the composite and neat resin samples are of similar shape but are translated along the temperature axis. In the high temperature region, the composite sample curve shows an approximately 5^{o} increase in position relative to the neat resin curve. In the low temperature region, the difference is smaller; the composite sample curve is displaced approximately 2.5^{o} below that of the neat resin. Crystallization rates of the APC-1 composite panel fell midway between the APC-2 composites and the neat resin. No difference was noted between the crystallization rates of the two APC-2 composite panels (GD432 and GD433) prepared at NASA.

Successive remeltings in the DSC (indicated under thermal history in the appendix) had no apparent affect on the crystallization behavior of either the PEEK composite or neat resin

Table III

PEEK - Isothermal Peak Positions

T_c (K)	Neat PEEK t_{max} (min)	APC-2 t_{max} (min)	APC-1 t_{max} (min)
430	19.1	8.55, 7.22	—
432.5	7.60, 7.9	4.33, 3.46	—
435	2.19, 3.69	1.98, 2.27	—
437.5	2.45	1.35	—
440	—	0.96, 0.84	—
570	1.20, 1.21	0.77	—
575	1.99	1.49, 1.50	1.71
580	3.43, 3.27 4.13	1.92, 2.02	2.51
585	5.95	3.95	4.85
590	15.8	6.47, 6.61	—
595	—	15	—

Fig. 3

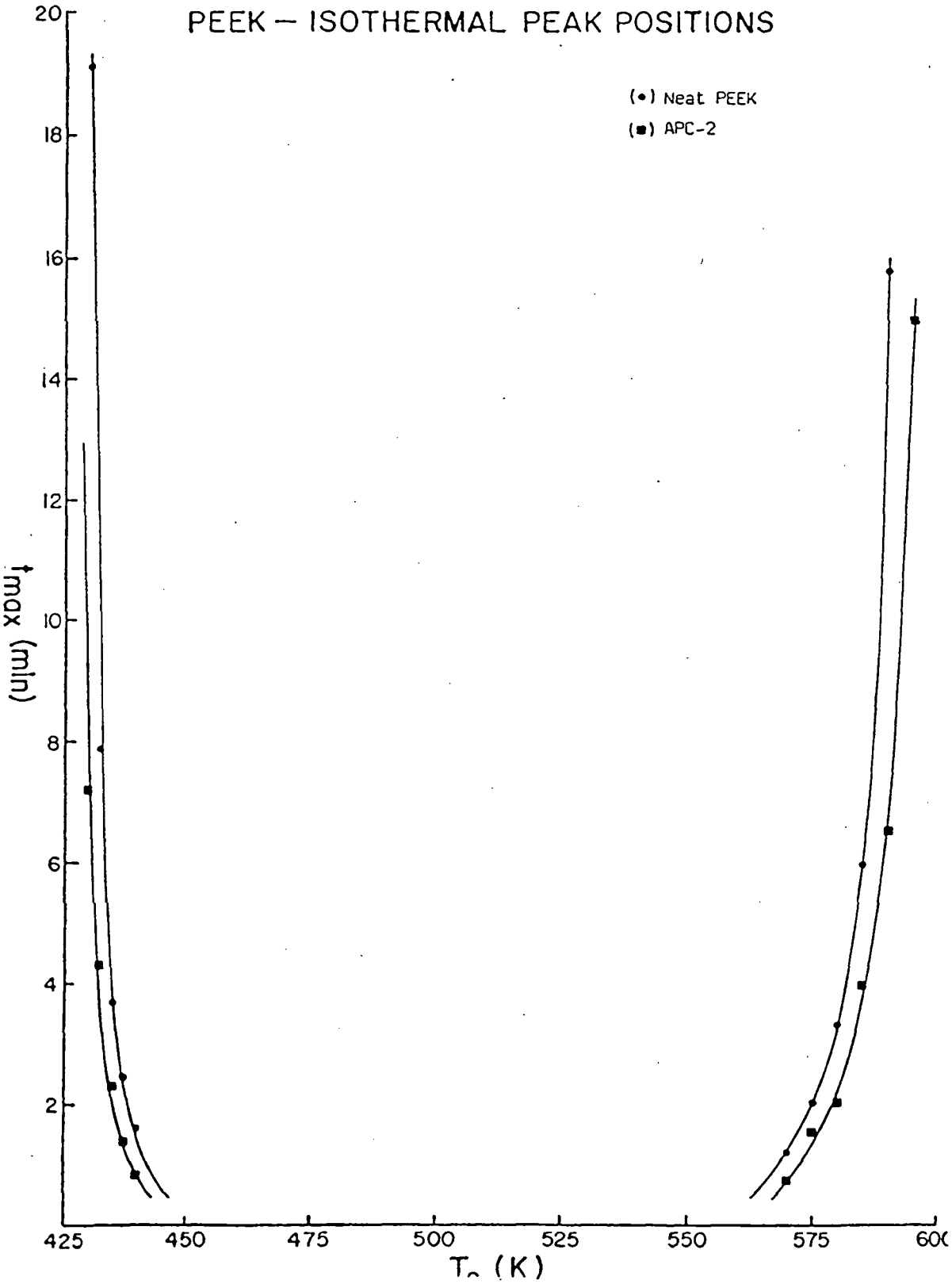
PEEK — ISOTHERMAL PEAK POSITIONS
(•) Neat PEEK
(■) APC-2
t_{max} (min)
T_a (K)
20
18
16
14
12
10
8
6
4
2
425
450
475
500
525
550
575
600

samples. Sample 01417, which was held at 680 K for two minutes before crystallization, behaved identically to sample 01416, which was held at the usual 670 K for two minutes before crystallization.

Degrees of crystallinity attained in the isothermal crystallizations of the neat PEEK and APC-2 composite samples, where polymer contents are known [25], are listed in the appendix. These values were calculated in the same manner as those for neat PPS. 130 J/g (31.0$_7$ cal/g) was used as the heat of fusion for a PEEK crystal [11]. Degrees of crystallinity attained in the isothermal crystallizations of the APC-2 composite samples appear to be approximately 7% higher than in neat PEEK for the high temperature crystallizations but with no appreciable difference in the low temperature crystallizations.

3.3 Crystallization Kinetics

Isothermal crystallization thermograms were analyzed using the Avrami method mentioned in section 1.8.

The time dependency of conversion during isothermal crystallization can be analyzed using equation 1.14

$$1 - Xc(t)/Xc(\infty) = \exp(-k't^n) \qquad (1.14)$$

Taking the natural log twice of each side of the above equation gives:

$$\ln[-\ln(1-c)] = \ln k' + n \ln t \qquad (3.1)$$

where c equals $Xc(t)/Xc(\infty)$.

If the crystallization follows the assumptions mentioned in the Avrami method, then plots of $\ln[-\ln(1-c)]$ vs. $\ln t$ should be linear with a slope of n and an intercept of $\ln k'$.

To illustrate the physical meaning of results obtained from crystallization kinetics analyses, three examples of isothermal crystallization thermograms yielding Avrami exponents of 2.59, 3.28, and 7.11, with their corresponding double logarithmic plots, are given in Fig. 4-6. From these thermograms it can be seen how the shapes of the energy flow curves relate to their corresponding Avrami exponents. Where the Avrami exponent is high, the crystallization abruptly rises to its maximum rate shortly after onset. Where the Avrami exponent is low, crystallization rate gradually increases; reaching its maximum long after onset. The double logarithmic plots are given in order to show visually the fit of the experimental data to this kind of

Fig. 4a

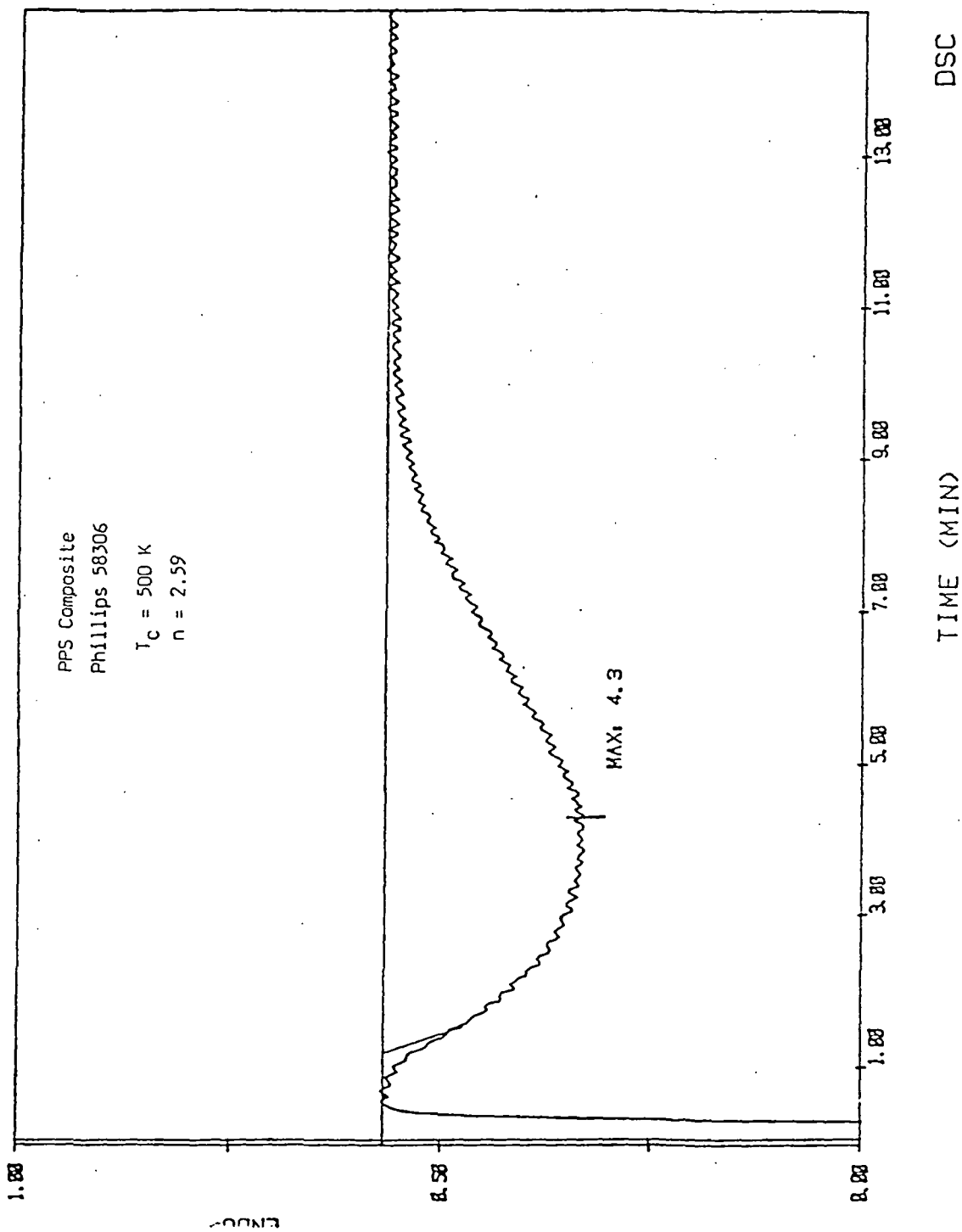
PPS Composite
Phillips 58306
T_c = 500 K
n = 2.59
MAX: 4.3
1.00
0.50
0.00
1.00
3.00
5.00
7.00
9.00
11.00
13.00
TIME (MIN)
DSC

Fig. 4b

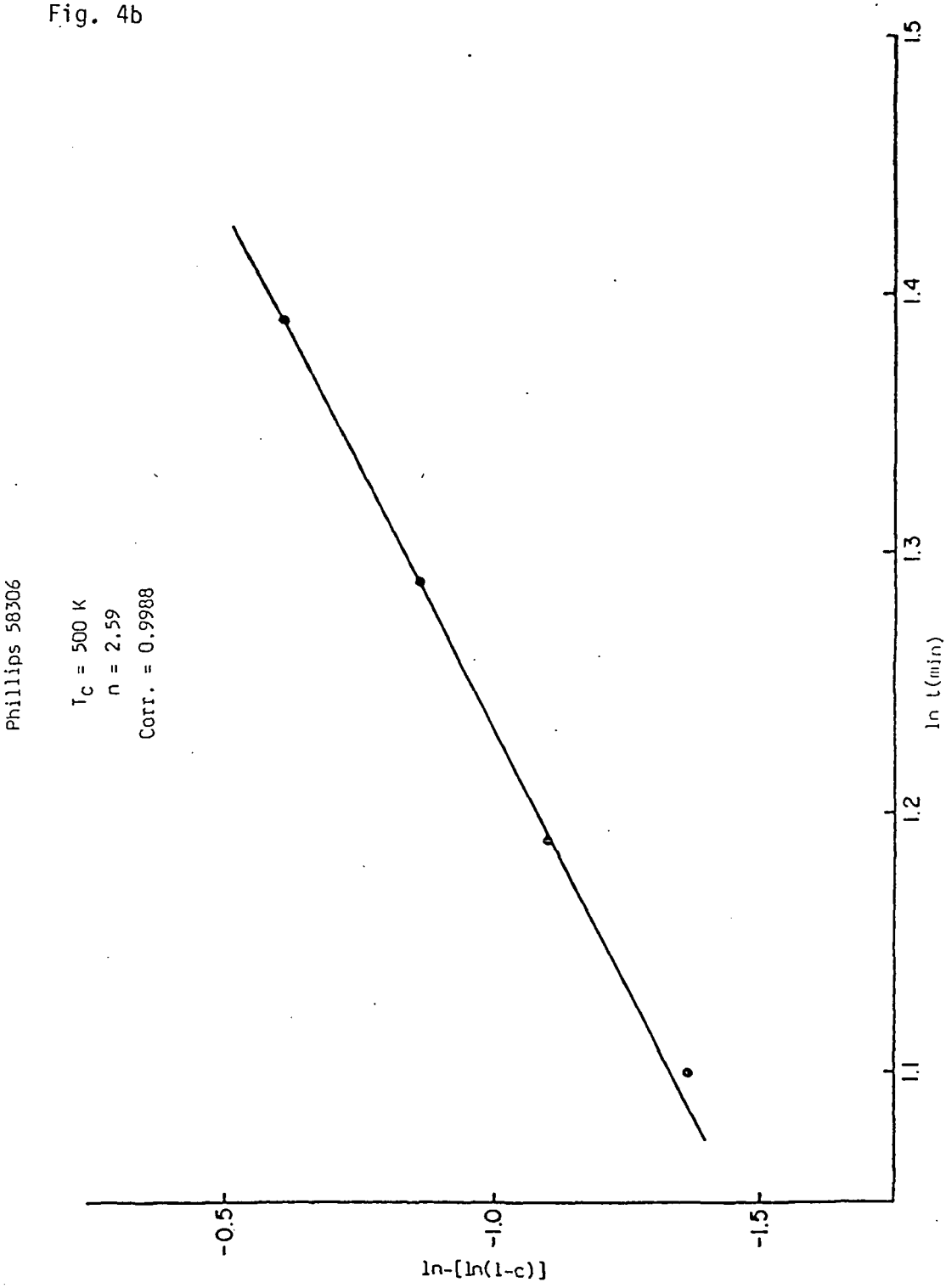
Phillips 58306
T_c = 500 K
n = 2.59
Corr. = 0.9988
-0.5
-1.0
-1.5
ln-[ln(1-c)]
1.1
1.2
1.3
1.4
1.5
ln t(min)

Fig. 5a

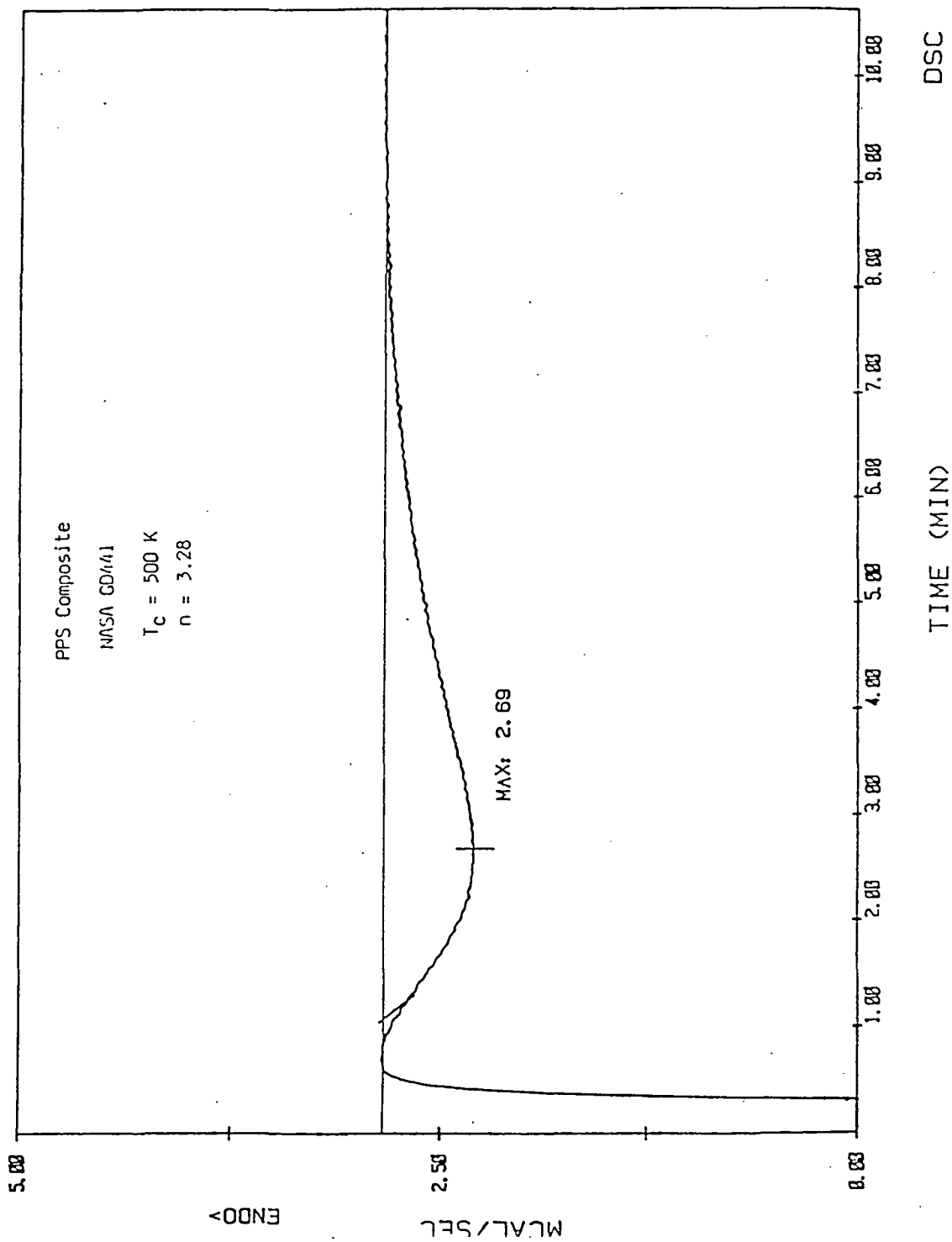
PPS Composite
NASA GD441
T_c = 500 K
n = 3.28
MAX: 2.69
MCAL/SEC
<ENDO>
5.000
2.500
0.000
1.000
2.000
3.000
4.000
5.000
6.000
7.000
8.000
9.000
10.000
TIME (MIN)
DSC

Fig. 5b

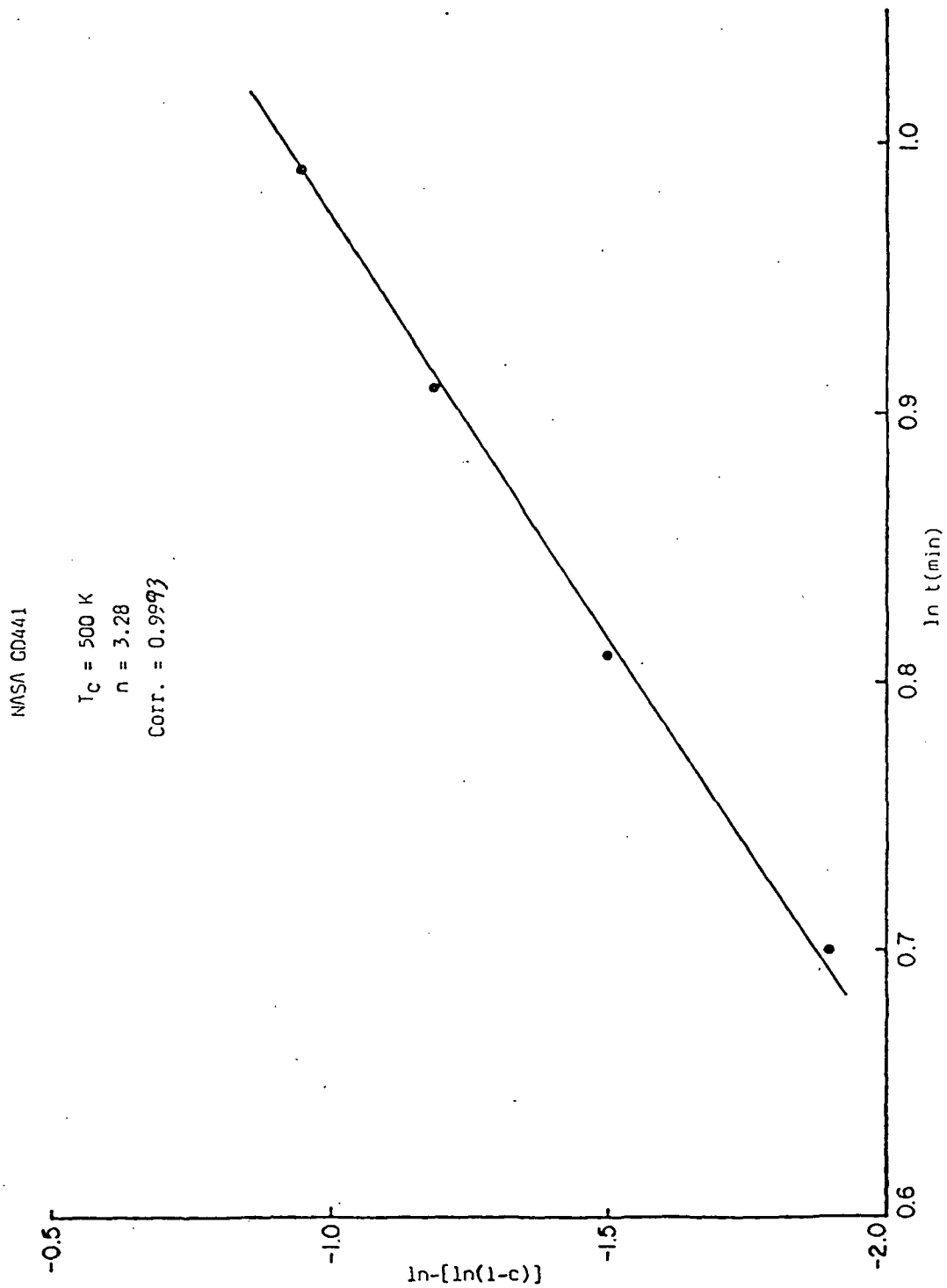
NASA GD441
T_c = 500 K
n = 3.28
Corr. = 0.9993
-0.5
-1.0
-1.5
-2.0
ln-[ln(1-c)]
0.6
0.7
0.8
0.9
1.0
ln t(min)

Fig. 6a

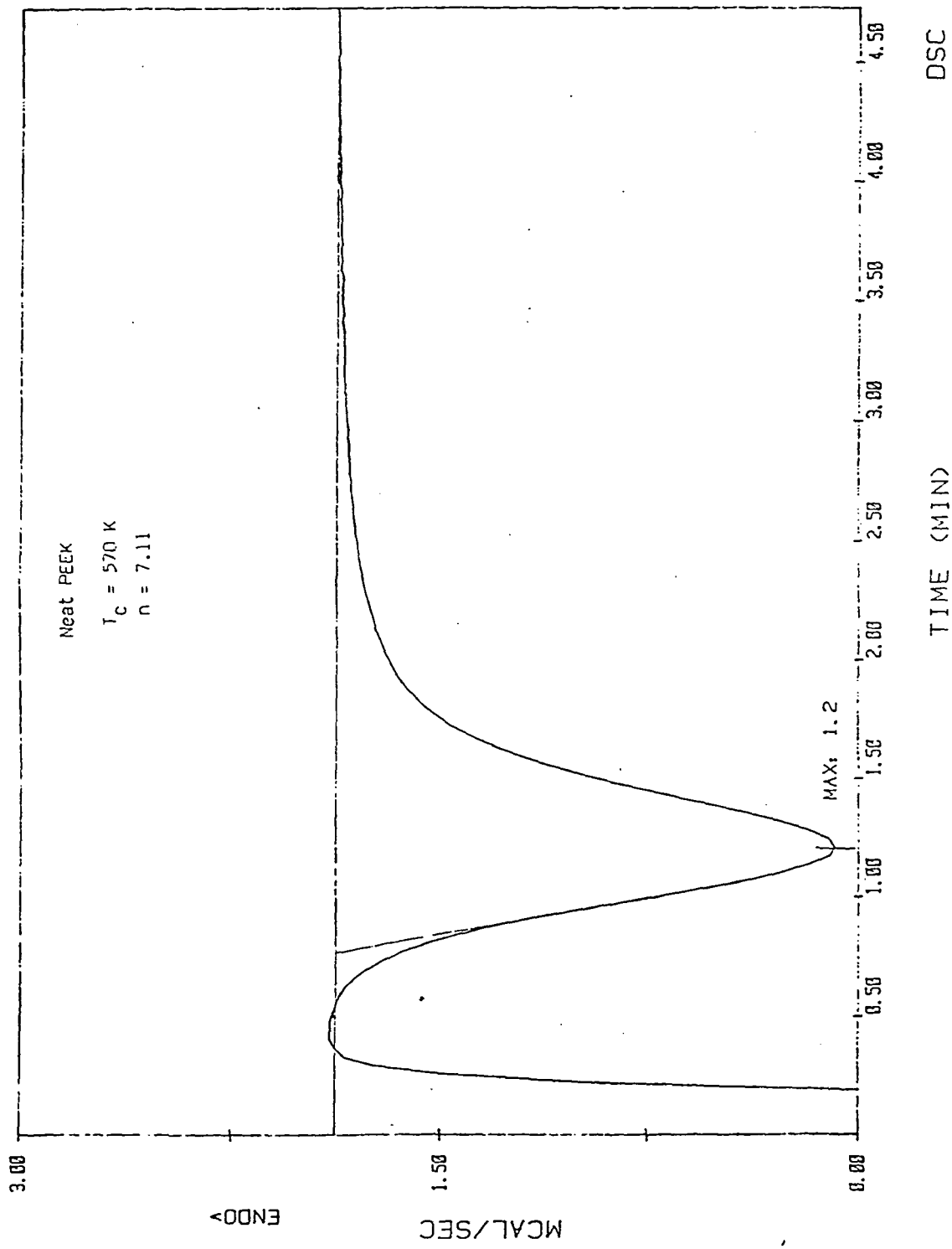
Neat PEEK
T_c = 570 K
n = 7.11
MAX: 1.2
3.00
1.50
0.00
ENDO>
MCAL/SEC
0.50
1.00
1.50
2.00
2.50
3.00
3.50
4.00
4.50
TIME (MIN)
DSC

Fig. 6b

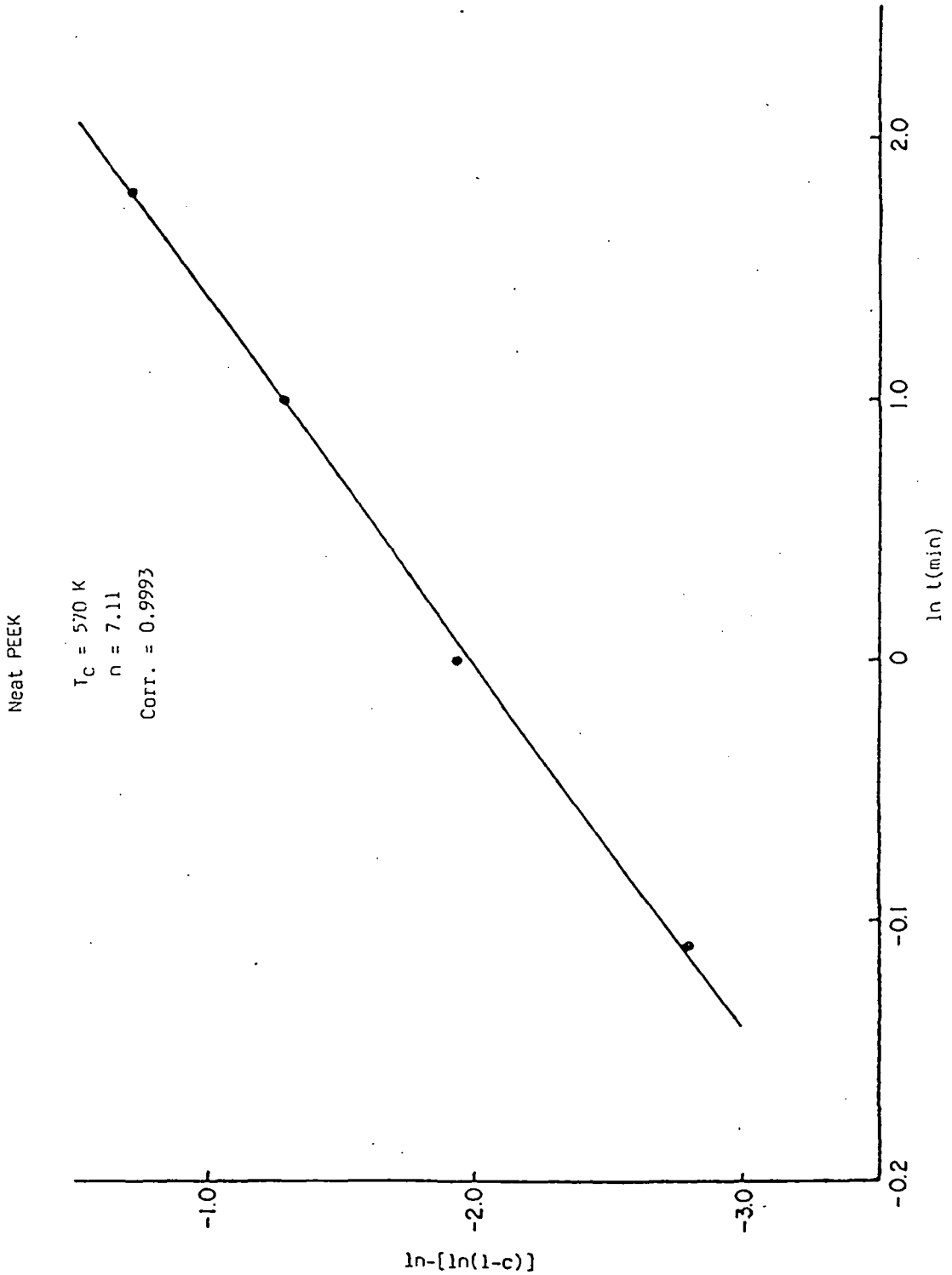
Neat PEEK
T_c = 570 K
n = 7.11
Corr. = 0.9993
ln-[ln(1-c)]
-1.0
-2.0
-3.0
ln t(min)
2.0
1.0
0
-0.1
-0.2

analysis together with their calculated correlation coefficients. All of the correlation coefficients are listed in the appendix.

3.4 Crystallization Kinetics - PPS

PPS isothermal crystallization thermograms were analyzed with respect to conversion levels at various times with the assistance of the model 3600 data station and the software provided by Perkin-Elmer.

Avrami plots of neat PPS and PPS composite samples showed a slight negative departure from linearity. This is believed to be due to the high degree of secondary crystallization which occurs in PPS. To minimize the effects of secondary crystallization on the Avrami analyses, only the initial portion of each thermogram was so analyzed. All thermograms were studied between the time limits of $0.75t_{max}$ to t_{max}. These limits corresponded to approximately 15-40% of the total conversion. Four data points were collected within these limits from each thermogram.

Values of n determined for the PPS composites and neat resin are listed in Table IV and are listed with their correlation coefficients in the appendix. Comparative plots of Avrami exponents are given in Fig. 7.

Table IV

PPS - Avrami Exponents

T_c (K)	Neat PPS n	NASA CD441 n	Phillips 58306 n
385	——	3.99	——
390	3.96,(5.36)	——	——
395	——	3.74	——
475	3.09	——	——
480	3.26	——	——
485	3.18, 3.04 (3.89)	——	——
490	3.08	3.38	——
495	——	3.43	2.66
500	3.08	3.28, 3.28 3.37,(5.23)	2.59
505	——	3.11	——
510	——	2.90, 3.10 (4.29)	——
515	——	3.38	——

Fig. 7

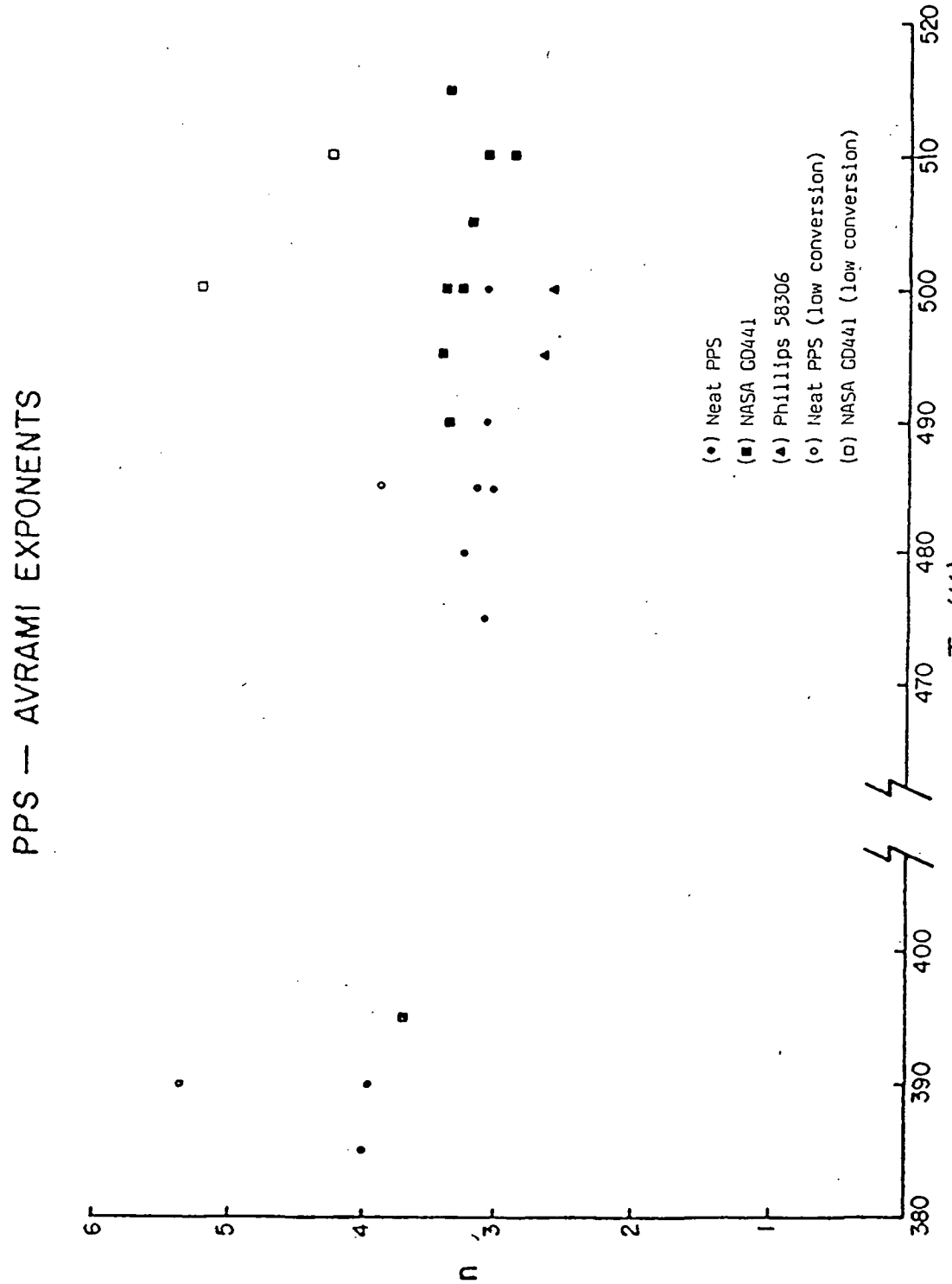
PPS — AVRAMI EXPONENTS
n
6
5
4
3
2
1
380
390
400
470
480
490
500
510
520
T_c (K)
(•) Neat PPS
(■) NASA CD441
(▲) Phillips 58306
(○) Neat PPS (low conversion)
(□) NASA CD441 (low conversion)

From the low temperature crystallizations, one neat resin and two NASA GD441 composite crystallization thermograms were determined to be suitable for analysis. Avrami exponents of just under 4 were found with no distinguishable difference between the neat resin and composite samples.

Among the high temperature isothermal crystallization data, DSC thermograms of six neat PPS resin samples, nine NASA GD441 PPS composite samples, and two Phillips 58306 PPS composite samples were determined to be suitable for analysis.

Avrami exponents determined from the six neat resin thermograms were highly consistent. They ranged from 3.04 through 3.26, and their average value was 3.11. The Avrami exponents found for the nine NASA GD441 composite thermograms were somewhat less consistent than those for the neat resin in that they ranged from 2.90 through 3.43. The average value of n for these composites was 3.25, which is similar to that found for the neat PPS resin. The two Phillips 58306 composite samples yielded Avrami exponents that were much lower those obtained for both the NASA composite and neat PPS resin samples. Values of n found from the two Phillips composite thermograms were 2.66 and 2.59.

3.5 Crystallization Kinetics of PPS - Early Stages

In an attempt to study the earliest part of the crystallization and thus eliminate effects of secondary crystallization, thermograms analyzed as described in Sec. 3.4 were reanalyzed at lower conversion levels. Four sets of crystallization data were chosen as suitable for reanalysis on the basis of their apparent baseline stability at the onset of crystallization. From the low temperature crystallizations, one thermogram of neat PPS resin sample crystallized at 390 K was chosen for reanalysis at low conversion level. From the high temperature crystallizations, one thermogram of a neat PPS resin sample crystallized at 485 K and two thermograms from the GD441 composite samples, crystallized at 500 and 510 K, were chosen for reanalysis. These thermograms were chosen for their apparent baseline stability at the onset of crystallization.

Limits over which these thermograms were reanalyzed included the early onset of crystallization to 0.75 t_{max}. These limits corresponded to approximately 2-15% of the total conversion.

Values of n determined for the PPS composite and neat resin samples at low conversion levels are listed in parentheses in Table IV and are listed in parentheses in the appendix underneath their corresponding values obtained at the standard conversion levels. Plots of Avrami exponents obtained at low conversion are also included in Fig. 7.

Avrami exponents obtained from the lower conversion level analyses varied greatly but were all much higher than their standard conversion level counterparts. They were from 0.85 - 1.95 higher than the values obtained at standard conversion levels. These higher exponents may be valid, but the great variation among them, their low correlation coefficients, and the small sampling of the overall crystallization exotherm make these analyses to appear to be less reliable than the ones of section 3.4.

3.6 Crystallization Kinetics - PEEK

Analyses of PEEK crystallization data in the manner suggested by the Avrami equation were carried out as stated for PPS. Values of n obtained for neat PEEK resin and composite samples are listed in Table V and are listed with their correlation coefficients in the appendix. Comparative plots of Avrami exponents are given in Fig. 8.

In the low temperature region, below T_{max}, Avrami analyses were carried out on four neat resin and four APC-2 composite sample crystallization thermograms. The values of n obtained for the four neat resin thermograms varied greatly, ranging from 3.61 to 5.27; their average was 4.40. Values of n obtained for the four APC-2 composite thermograms below T_{max} also showed great variance, averaging 3.88 but ranging from 3.01 to 4.71.

Table V

PEEK - Avrami Exponents

T_c (K)	Neat PEEK n	APC-2 n	APC-1 n
430	4.20	3.88	—
432.5	3.61	4.71	—
435	4.51	4.41	—
437.5	5.27	—	—
570	7.11, 6.98	—	—
575	7.14	—	3.64
580	5.77	3.69, 3.81	3.44
585	—	—	4.29
590	—	3.51	3.75

Fig. 8

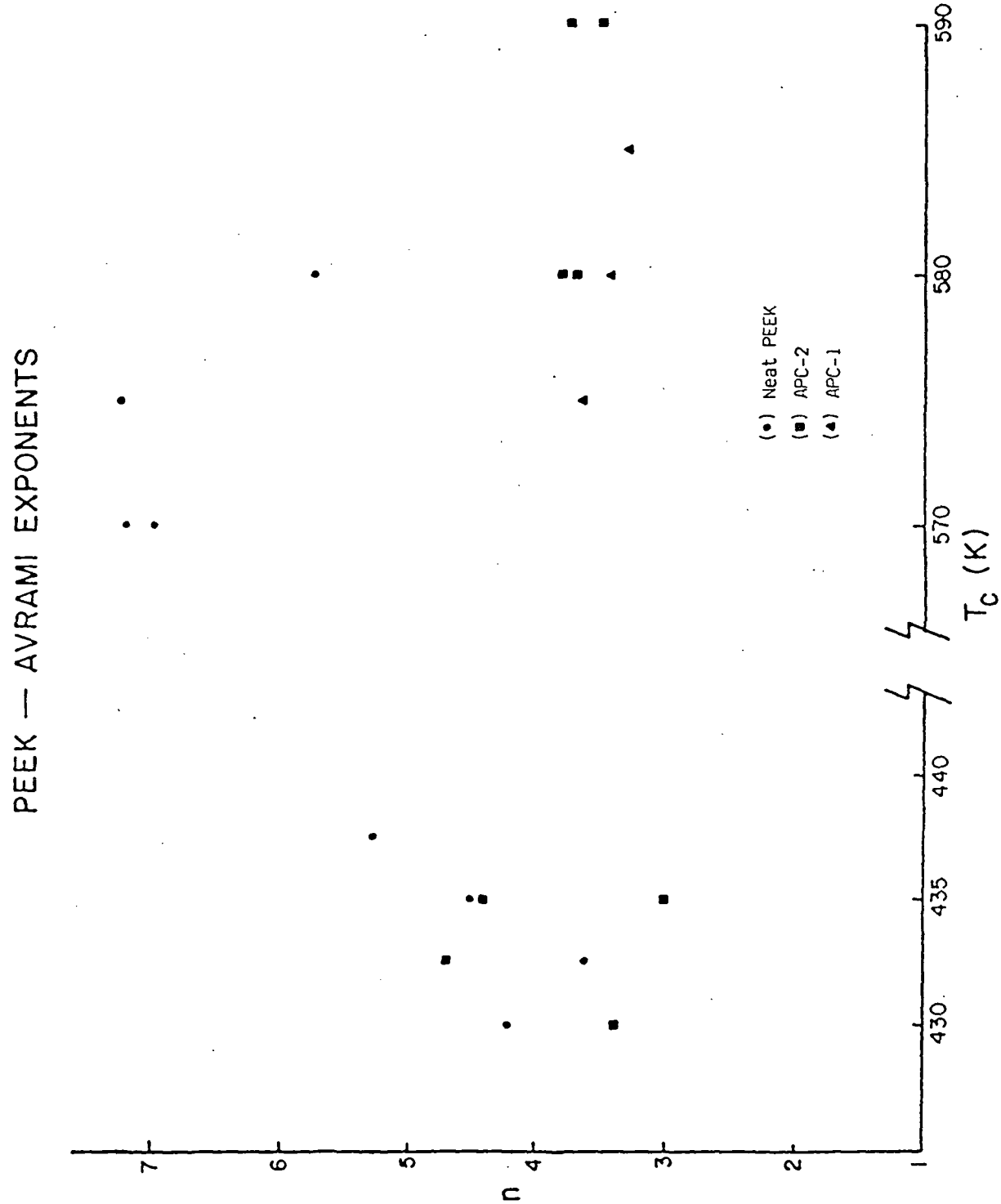
PEEK — AVRAMI EXPONENTS
(•) Neat PEEK
(■) APC-2
(▲) APC-1
n
T_c (K)
1
2
3
4
5
6
7
430
435
440
570
580
590

In the high temperature range, these analyses were carried out on four neat PEEK resin, four APC-2 composite, and three APC-1 composite sample crystallization thermograms.

The values of n obtained for the neat PEEK resin in the high temperature region ranged from 5.77 to 7.14, yielding an average value of 6.75. These exponents are much higher than those commonly found in crystallizable polymer systems.

The four isothermal crystallizations of APC-2 composite samples yielded n values ranging from 3.51 to 3.81 and averaged 3.69. Values of n obtained for the three APC-1 composite samples ranged from 3.44 to 4.29 and averaged 3.79. There was a greater variation in Avrami exponents for the APC-1 than for the APC-2 composites, but the averages of the two groups were similar.

3.7 T_m^* vs. T_c Analysis of PEEK

Isothermally crystallized neat PEEK and PEEK composite samples displayed dual melting endotherms. Each melting thermogram included a primary peak that was larger and found at higher temperatures than the secondary melting peak. Melting thermograms for neat PEEK crystallized at different temperatures are plotted together in Fig. 9 and those for the APC-2 composite in Fig. 10. Temperatures of peak maxima were determined using the Perkin-Elmer 3600 data station. These data from each thermogram are listed in Table VI. These temperatures have been corrected

Fig. 9

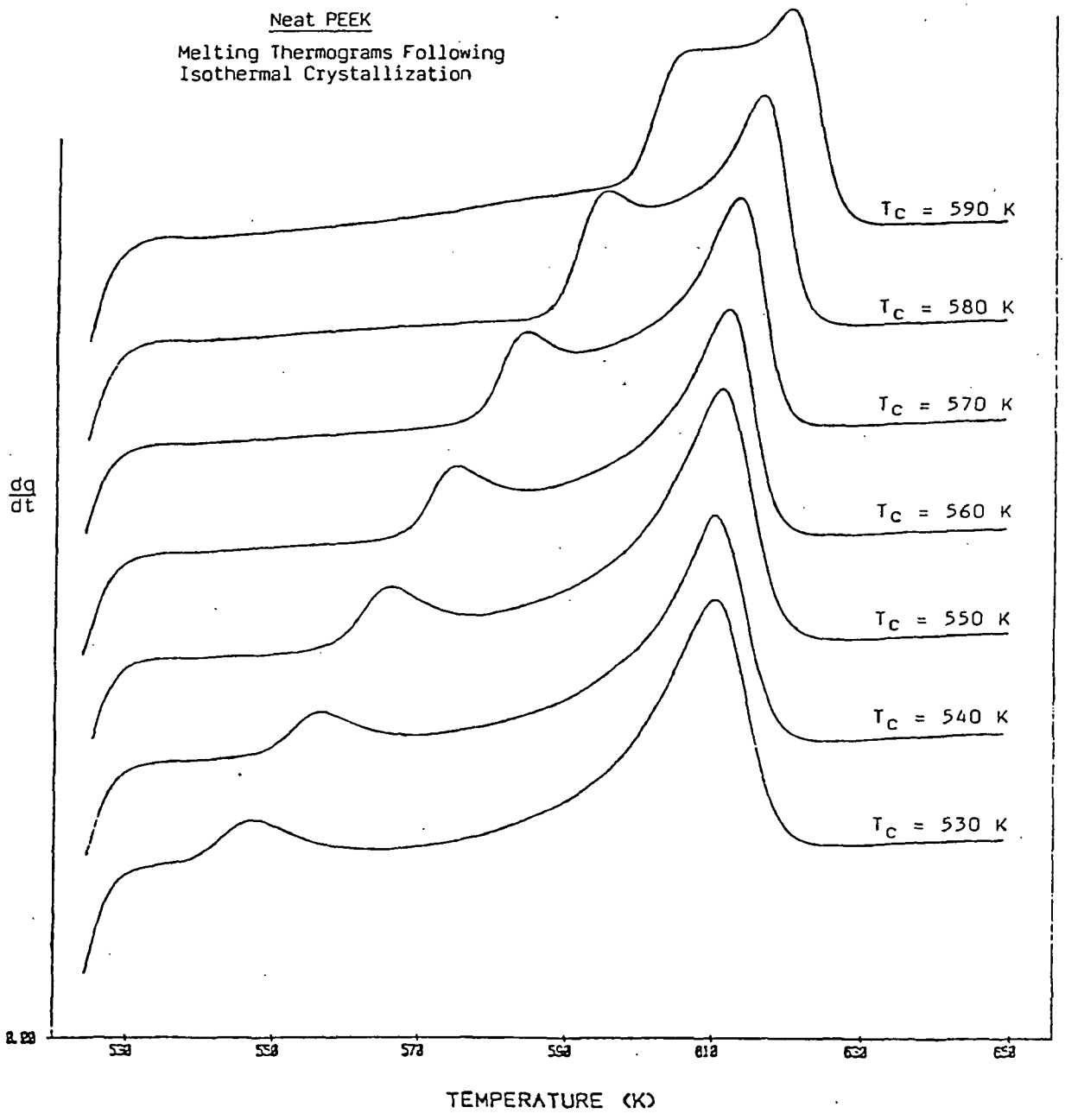
Neat PEEK
Melting Thermograms Following
Isothermal Crystallization
T_c = 590 K
T_c = 580 K
T_c = 570 K
T_c = 560 K
T_c = 550 K
T_c = 540 K
T_c = 530 K
dq/dt
TEMPERATURE (K)

Fig. 10

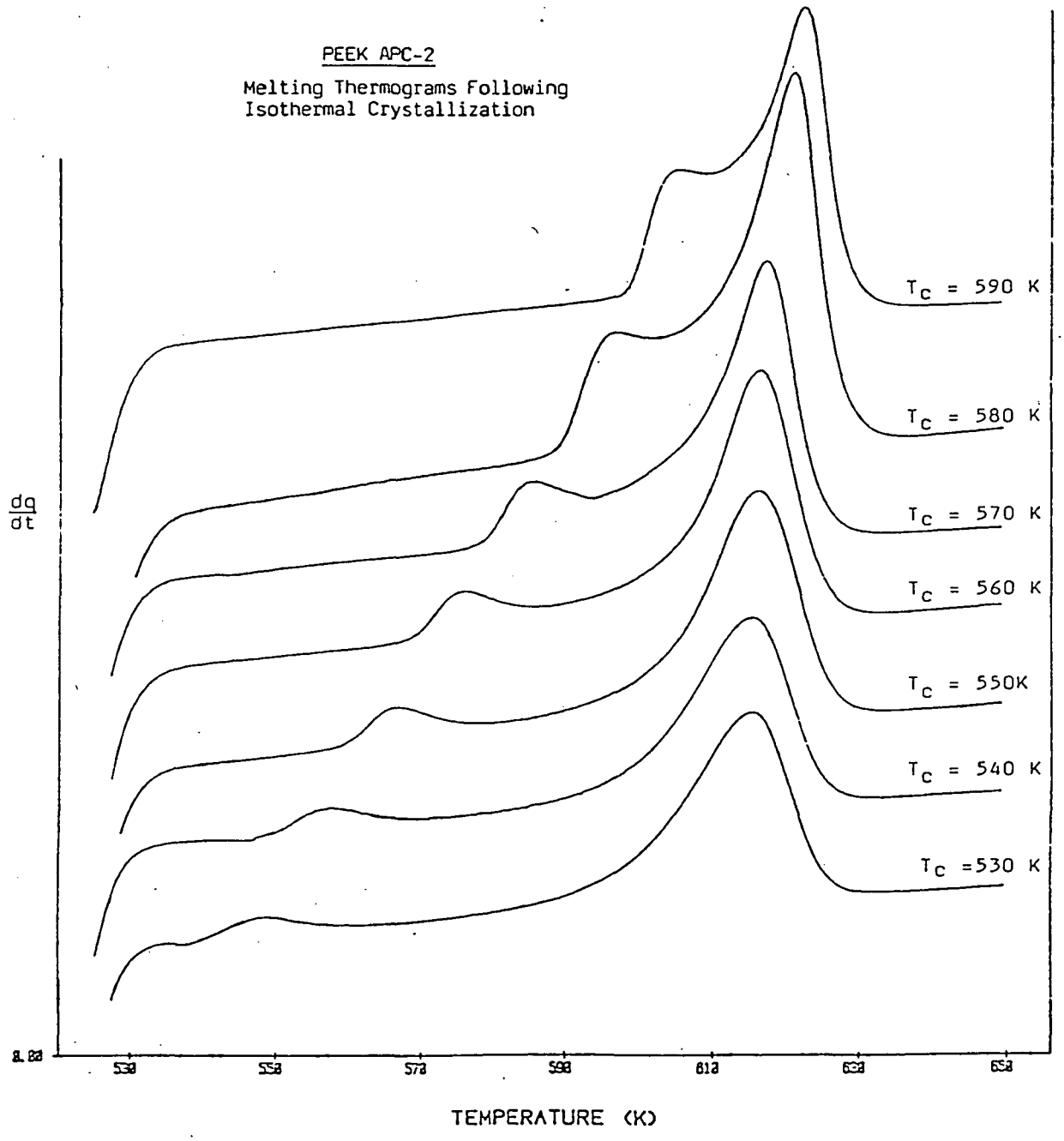
PEEK APC-2
Melting Thermograms Following
Isothermal Crystallization
T_c = 590 K
T_c = 580 K
T_c = 570 K
T_c = 560 K
T_c = 550K
T_c = 540 K
T_c =530 K
dq/dt
TEMPERATURE (K)

Table VI

PEEK - T_m^* vs. T_c

	Neat PEEK		APC-2	
T_c (K)	T_m^*(low)	T_m^*(high)	T_m^*(low)	T_m^*(high)
532.3	544.9	608.0	546.2	613.4
542.3	554.1	608.1	555.1	613.1
552.3	563.6	609.3	564.3	614.1
			565.0	616.0 -(low mass)
			564.3	614.3 -(680K)
562.3	572.3	609.6	573.3	614.4
572.3	581.8	611.2	582.3	615.3
582.3	592.1	614.1	592.7	618.5
592.3	602.5	617.8	601.4	620.3

with respect to heating rate. Plots of T_m* vs T_c for neat PEEK and PEEK composite samples are given in Fig. 11.

The temperatures of the primary melting peaks are fairly constant over the temperature range studied, but a gradual increase occurs beginning at the higher crystallization temperatures. A difference in the primary peak positions was noted between the neat PEEK and the PEEK composites. The position of the primary melting peak in neat PEEK samples was approximately 4° lower than in the PEEK composites over most of the crystallization temperature range studied. Thermograms of a PEEK composite sample and a neat PEEK sample, both crystallized at 550 K, were plotted together for comparison (Fig. 12).

The melting data in Table VI that were marked low mass were obtained from a sample that was about one-half the mass of the other composite samples. This sample had melting peak positions similar to those of the other composite samples. This indicates that the higher temperatures of the primary peaks found for the composites relative to the neat PEEK samples could not derive from thermal lag due to the larger sample sizes of the composites vs. the neat PEEK samples used in the study.

Positions of the secondary melting peaks were not constant over the temperature range studied; they increased linearly with crystallization temperature with a slope of about 0.9. No

Fig. 11

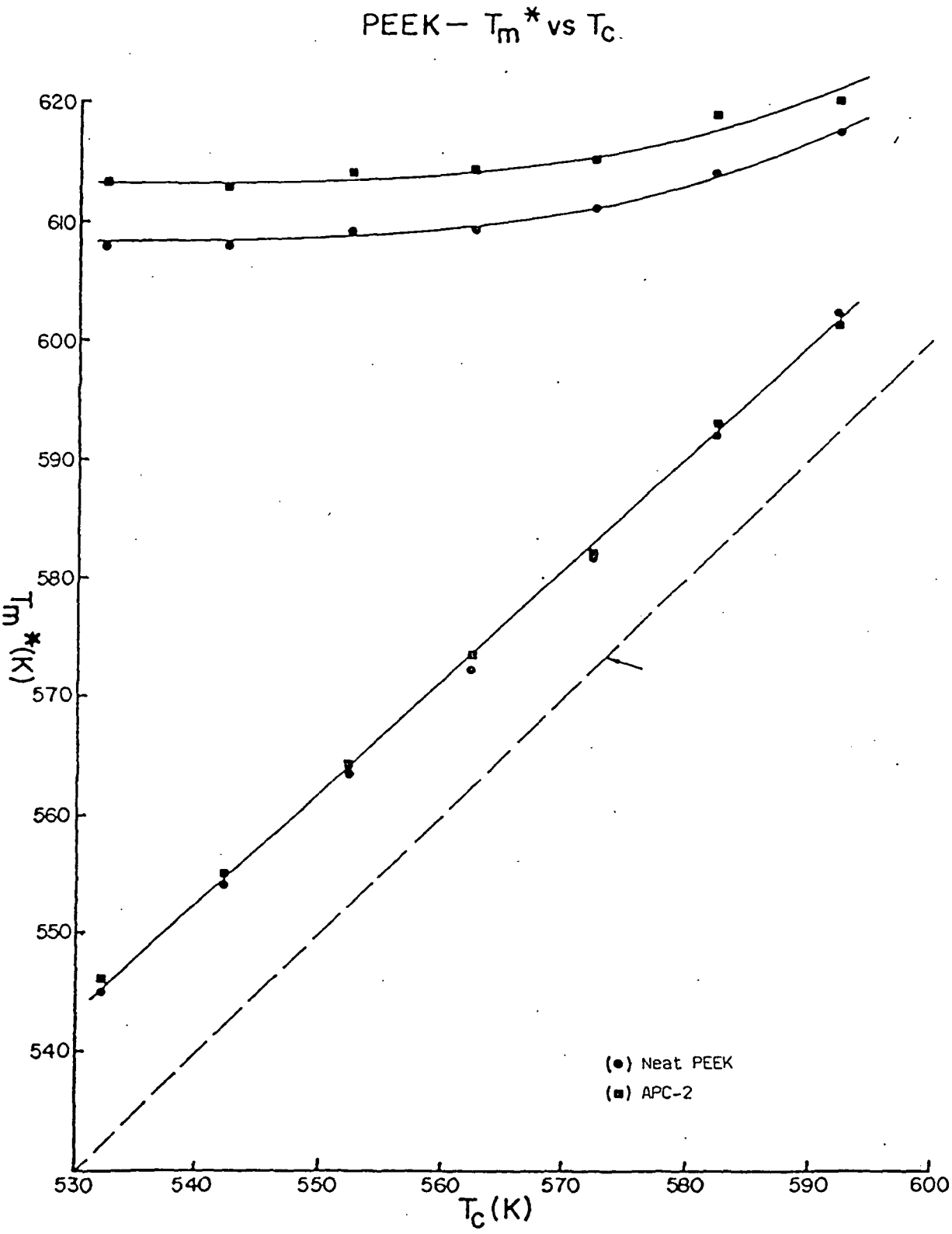
PEEK— T_m* vs T_c
620
610
600
590
580
570
560
550
540
T_m*(K)
530
540
550
560
570
580
590
600
T_c (K)
(●) Neat PEEK
(■) APC-2

Fig. 12

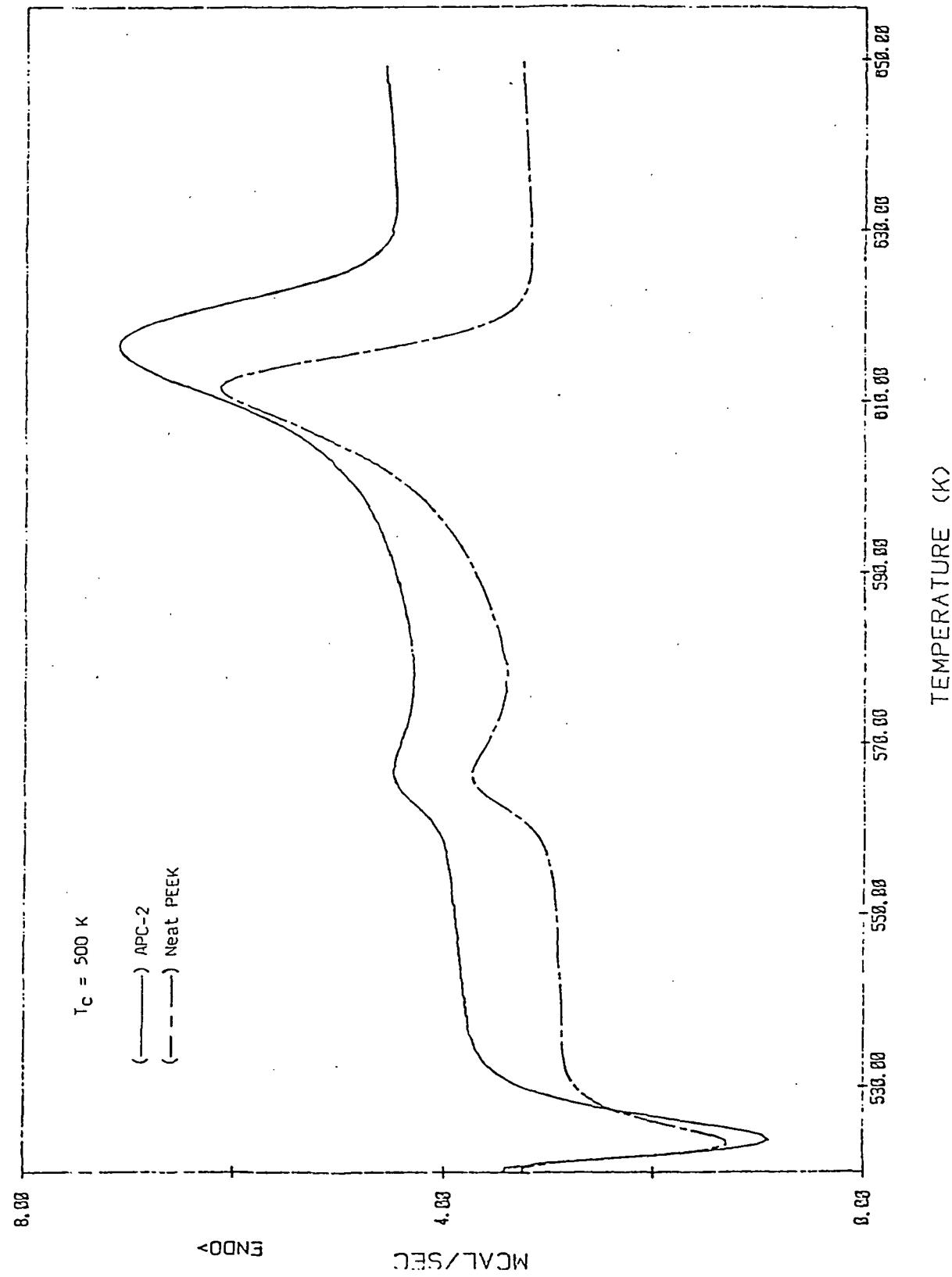
T_c = 500 K
(———) APC-2
(— - —) Neat PEEK
8.00
4.00
0.00
MCAL/SEC
<ENDO
530.00
550.00
570.00
590.00
610.00
630.00
650.00
TEMPERATURE (K)

significant difference was noted in the secondary peak position between the neat PEEK and PEEK composite samples.

The melting data of Table VI marked 680 K were obtained from a sample that was held at 680 K for two minutes before crystallization. It behaved identically to the composite samples held at the usual 670 K for two minutes before crystallization, indicating that sufficient premelting had occurred in the latter samples.

3.8 PEEK - T_m^* vs. T_c (partial crystallization)

Heating thermograms of the neat PEEK sample, which was partially and totally crystallized at 585 K (section 2.6) are given in Fig. 13. The total area of each endothermic peak was measured and peak maxima temperatures were determined. The degree of relative conversion in the partially crystallized sample was determined to be 28%. This value was calculated by dividing the heat of fusion of the partially crystallized sample by the heat of fusion of the fully crystallized sample.

The fully crystallized sample displayed both primary (high temperature) and secondary (low temperature) melting peaks. The partially crystallized sample showed only the primary peak.

Fig. 13

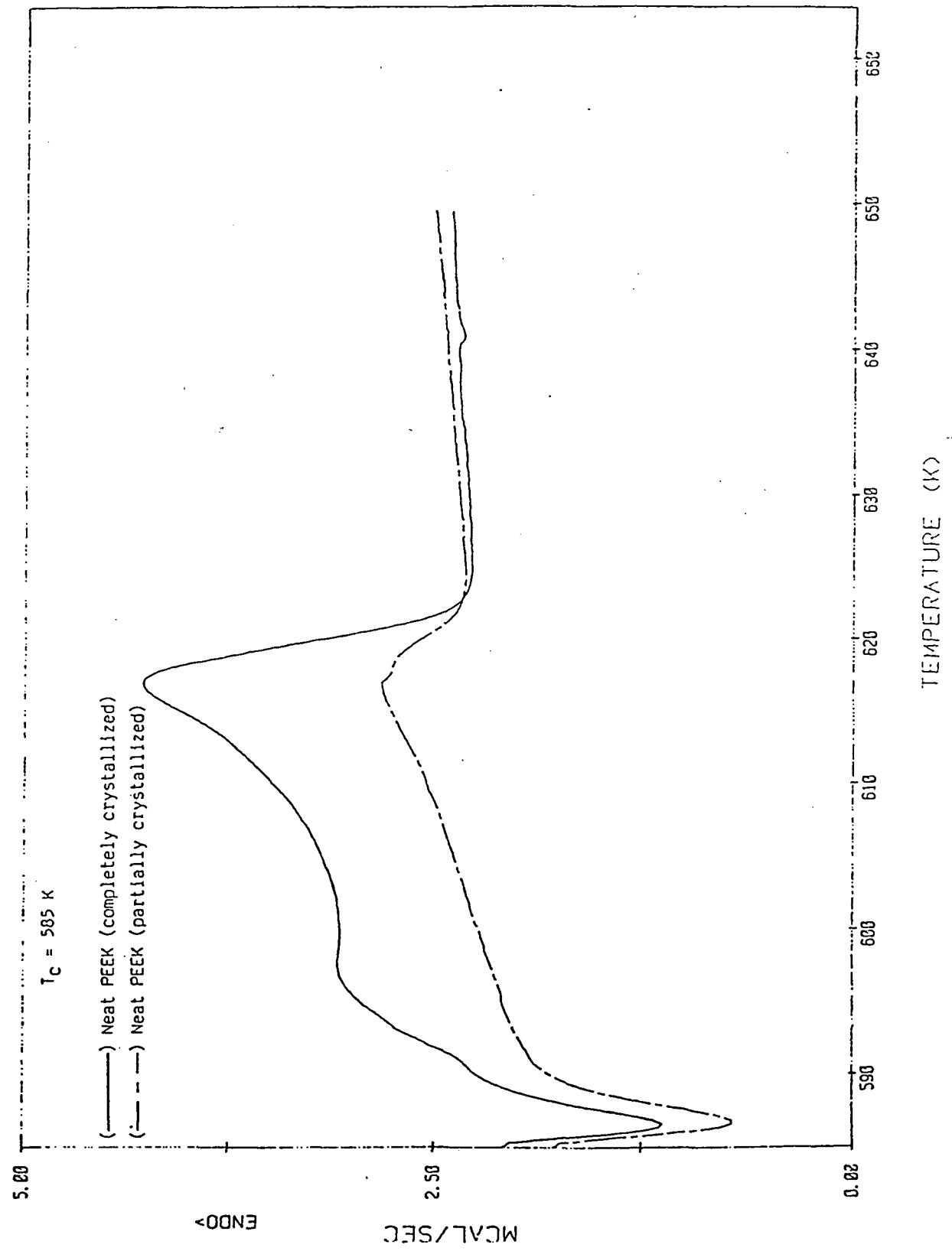
5.00
2.50
0.02
MCAL/SEC
ENDO>
590
600
610
620
630
640
650
652
TEMPERATURE (K)
T_c = 585 K
(——) Neat PEEK (completely crystallized)
(— — —) Neat PEEK (partially crystallized)

This indicates that the crystallinity corresponding to the secondary melting peak occurs from the crystallinity forming late in the crystallization and is, therefore, indicative of secondary crystallization. Wunderlich previously found that the lower melting temperature crystals form first [7]. This experiment was carried out to confirm that finding and later relate it to PPS.

3.9 T_m^* vs. T_c Analysis of PPS

Results of the T_m^* vs. T_c analyses of PPS were qualitatively identical to the results obtained with PEEK. Dual melting endotherms were observed for isothermally crystallized neat PPS and PPS composite samples. As in PEEK, each melting thermogram consisted of a primary and secondary melting peak. The primary melting peaks were larger and occurred at higher temperatures than did the secondary melting endotherms. Melting thermograms for neat PPS and PPS composite samples are give in Fig. 14 and Fig. 15 respectively. Peak positions in each thermogram are listed in Table VII. Temperatures have been corrected with respect to heating rate. Plots of T_m^* vs. T_c for neat PPS and PPS composite samples are given in Fig. 16.

As in PEEK, the temperatures of the primary melting peaks in PPS are fairly constant over the temperature range studied, but

Fig. 14

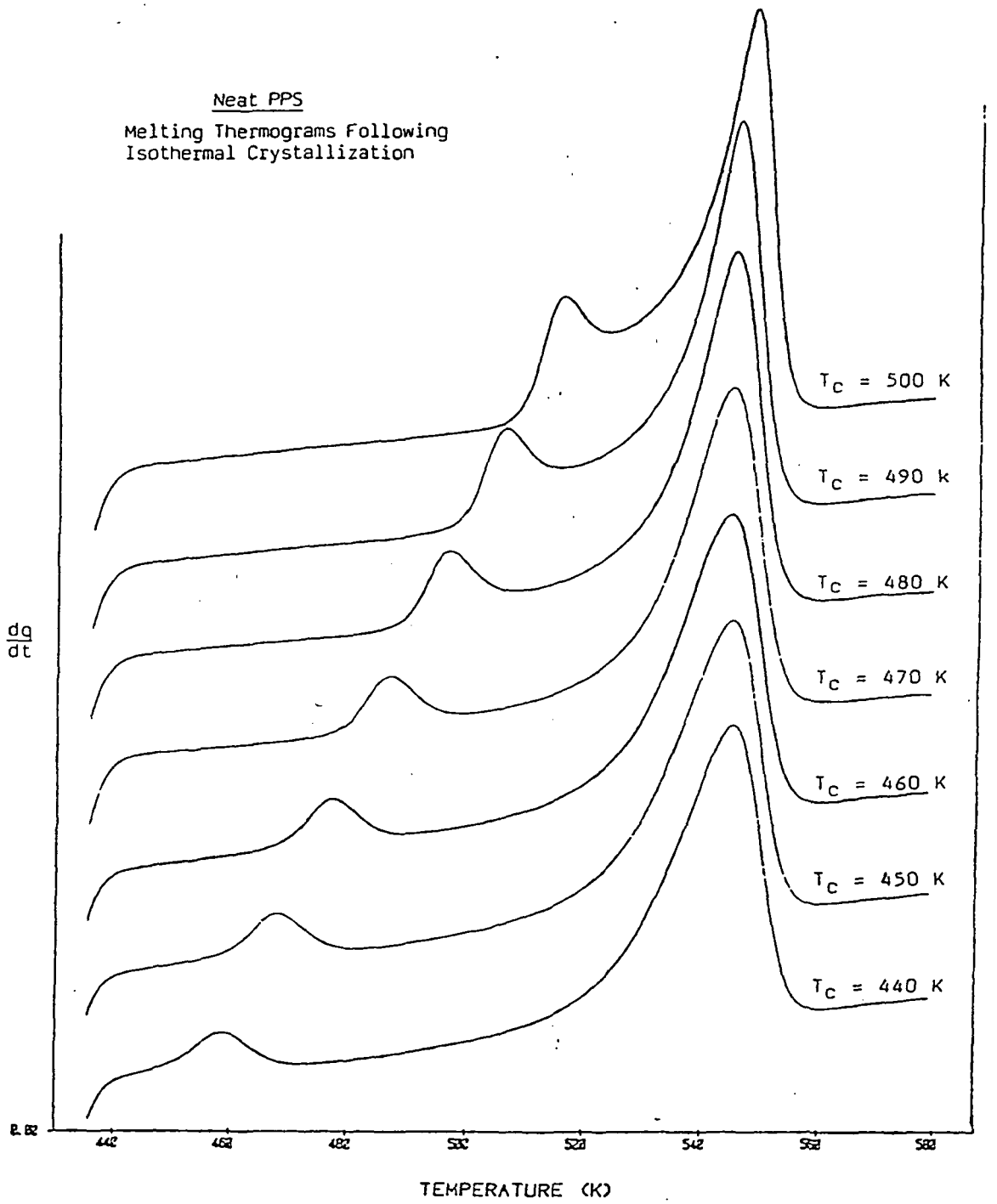
Neat PPS
Melting Thermograms Following
Isothermal Crystallization
T_c = 500 K
T_c = 490 k
T_c = 480 K
T_c = 470 K
T_c = 460 K
T_c = 450 K
T_c = 440 K
dq/dt
TEMPERATURE (K)

Fig. 15

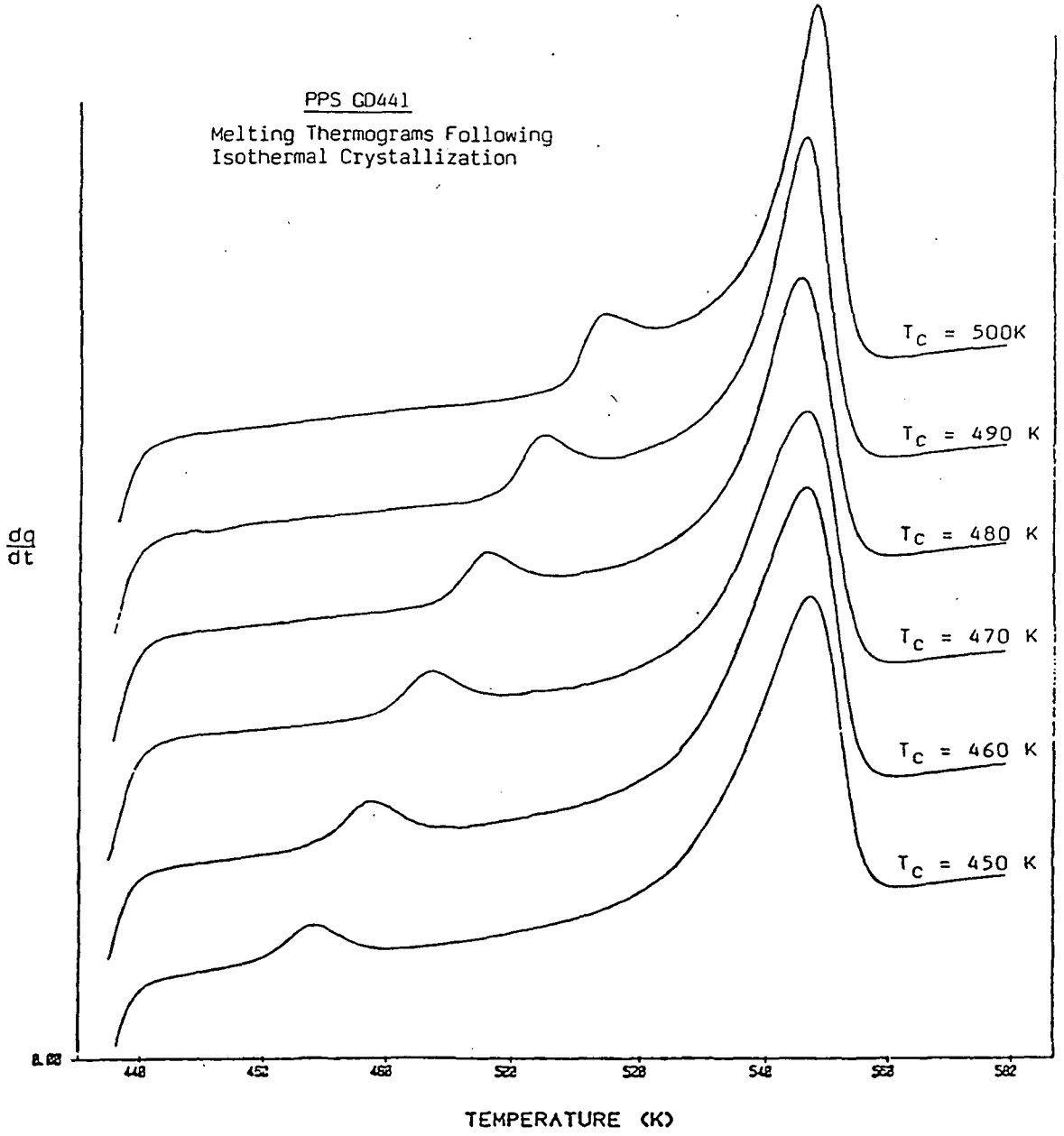
PPS GD441
Melting Thermograms Following
Isothermal Crystallization
T_c = 500K
T_c = 490 K
T_c = 480 K
T_c = 470 K
T_c = 460 K
T_c = 450 K
dq/dt
TEMPERATURE (K)

Table VII

PPS - T_m* vs. T_c

	Neat PPS		GD441	
T_c (K)	T_m*(low)	T_m*(high)	T_m*(low)	T_m*(high)
442.3	456.2	543.2	456.3	545.3
452.3	465.7	542.9	465.8	545.0
462.3	474.6	542.2	475.3	544.5
472.3	484.1 484.4	542.0 542.3	484.5 484.7	543.8 544.1
482.3	494.3	542.7	493.8	543.6
492.3	503.8	543.8	502.8	544.4
502.3	513.3	545.9	512.3	546.2

Fig. 16

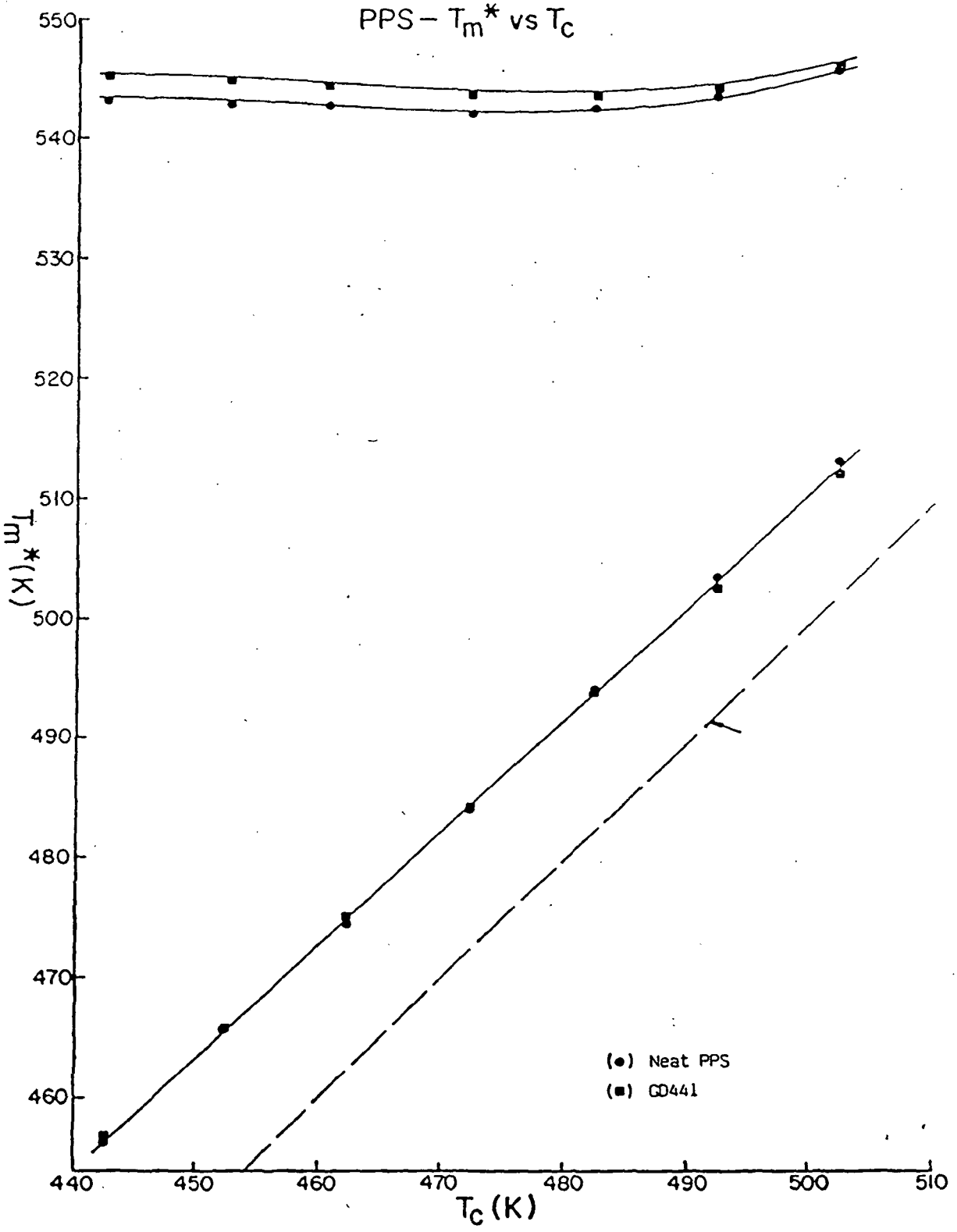
PPS – T_m* vs T_c
550
540
530
520
510
500
490
480
470
460
T_m*(K)
440
450
460
470
480
490
500
510
T_c (K)
(●) Neat PPS
(■) GD441

a gradual increase begins at the higher crystallization temperatures. However, for PPS, a slight increase in primary peak position was also noted at the lower crystallization temperatures. The differences in the primary peak positions between the neat PPS and the PPS composites were not as great as noted for PEEK. They were approximately 2^{o} lower for the neat PPS samples than for the PPS composites over most crystallization temperatures studied. Thermograms of a PPS composite sample and a neat PPS sample, both crystallized at 470 K, were plotted together for comparison (Fig. 17).

As for PEEK, positions of the secondary melting peaks for PPS increased linearly with crystallization temperature with a slope of about 0.9, and no difference in the secondary peak positions between neat PPS and PPS composite samples was noted.

PPS samples that were thermally cycled four times, then crystallized at 470 K, behaved identically to samples melted only once then crystallized at 470 K. This indicates that the thermal stability of the PPS samples was not a factor in this set of experiments.

3.10 PPS - T_m^* vs. T_c (partial conversion)

Heating thermograms of the neat PPS sample which was both partially and totally crystallized at 485 K (section 2.8) were plotted together in Fig. 18. The total area of each endothermic

Fig. 17

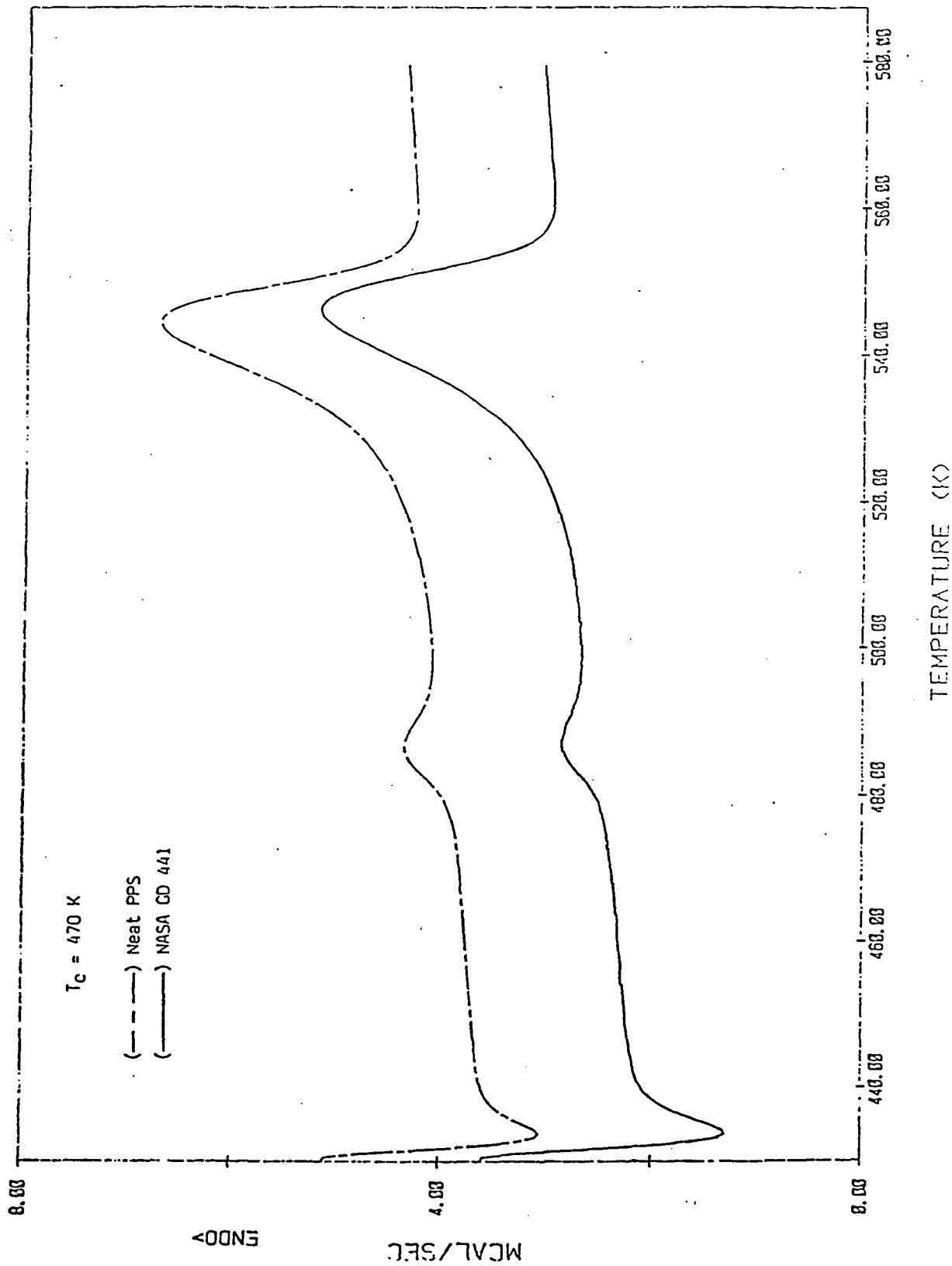
8.00
4.00
0.00
ENDO>
MCAL/SEC
440.00
460.00
480.00
500.00
520.00
540.00
560.00
580.00
TEMPERATURE (K)
T_c = 470 K
(— — —) Neat PPS
(———) NASA CD 441

Fig. 18

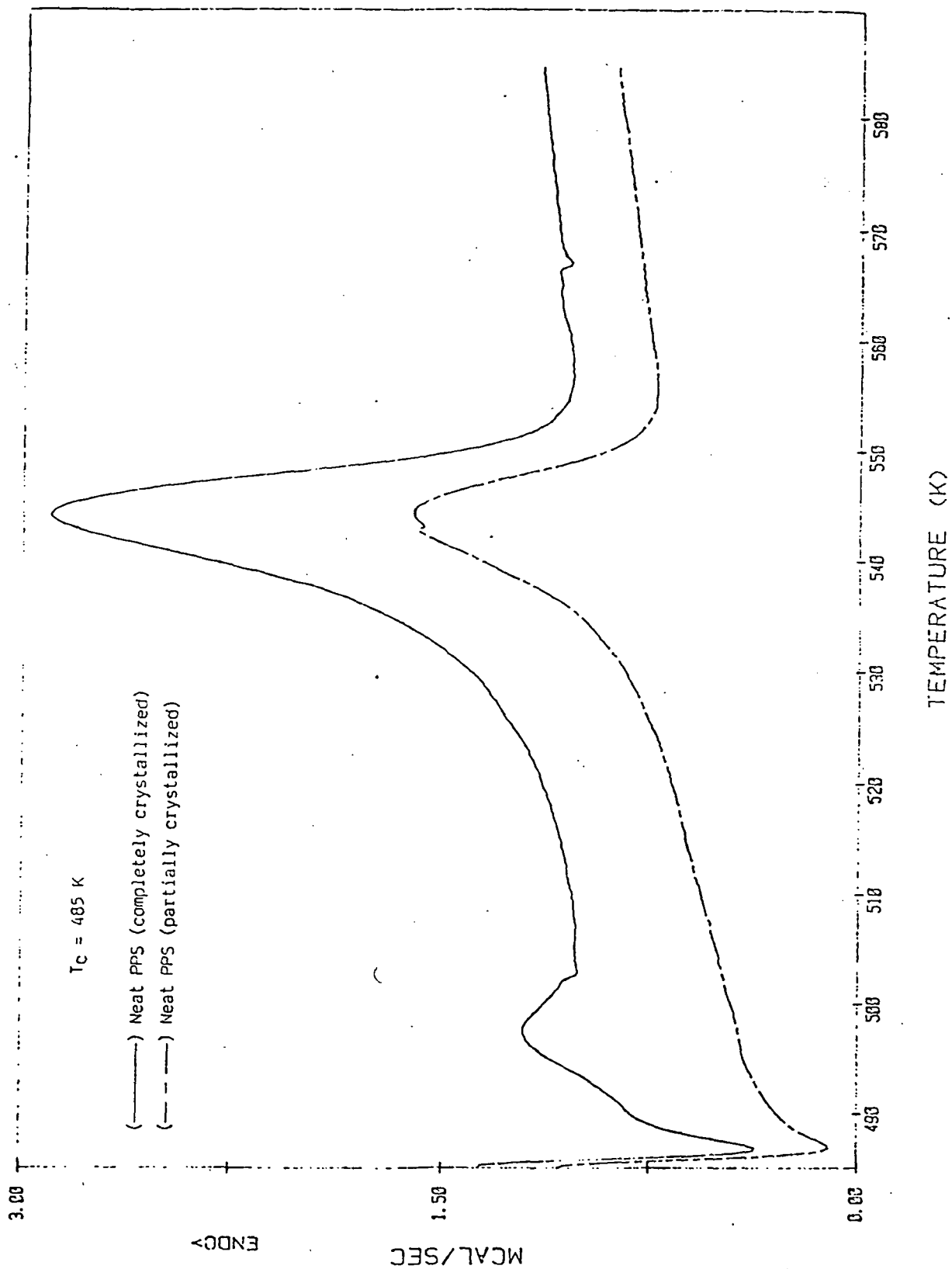

peak was measured, and the temperatures of the peak maxima were determined. The relative degree of conversion in the partially crystallized sample was determined to be 65%.

As in PEEK, the fully crystallized PPS sample showed both primary and secondary melting peaks, and the partially crystallized sample displayed only the primary peak. This indicates that the secondary melting peak in PPS occurs from the crystallinity forming late in the crystallization and is, therefore, indicative of secondary crystallization.

3.11 Microscopy

Quenched PEEK films containing low areal densities of carbon fibers were observed under a polarizing microscope with a first-order red retardation plate in place. The films displayed extensive birefringence, and the birefringent colors were partitioned into differently colored zones by the carbon fibers (Fig. 19a). The sample was subsequently crystallized at 440 K under a polarizing microscope using a Mettler FP-2 Microscope Hot Stage. Birefringent colors in the crystallized sample were not as deep as in the amorphous sample, yet distinct orientation of the polymer could be seen in the proximity of the the carbon fibers (Fig. 19b).

PEEK films from which fibers had been omitted showed slight birefringence with large areas showing general orientation.

Fig. 19

PEEK

a

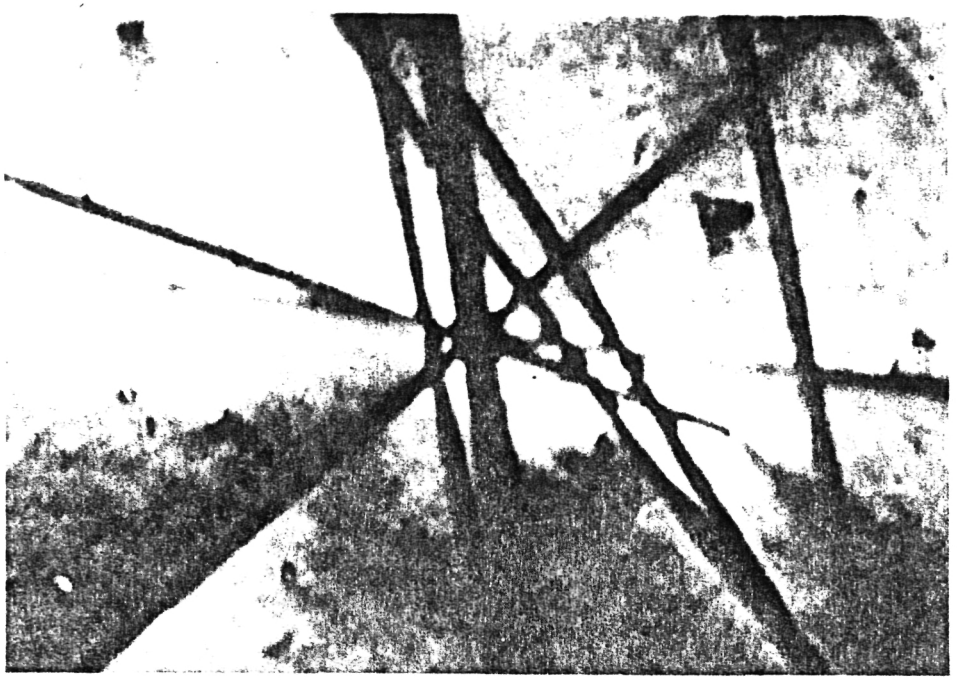

Quenched-amorphous PEEK film with carbon fibers

b

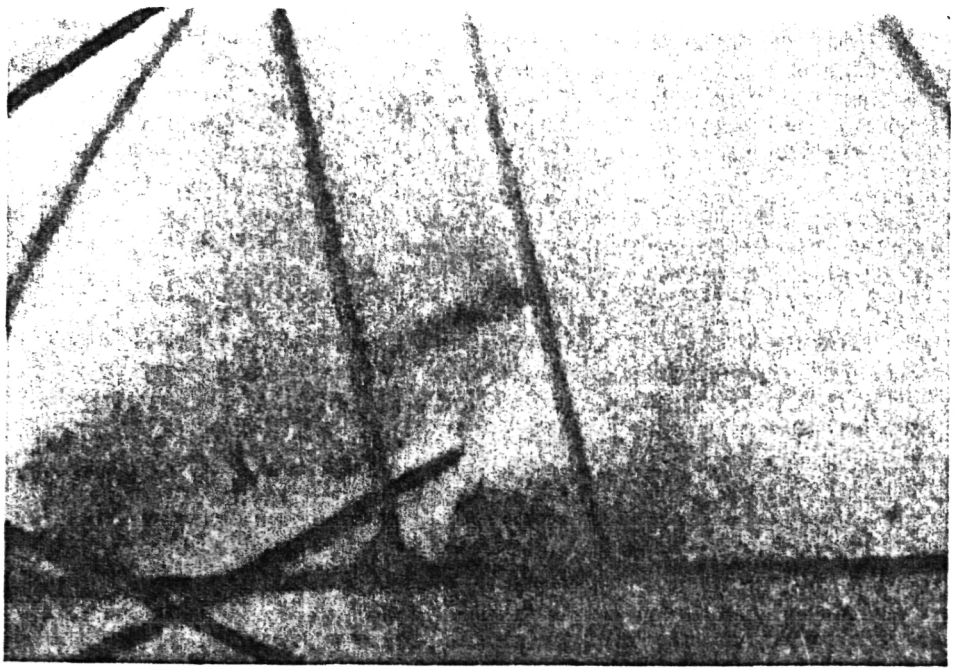

The above film crystallized at 440 K.

This is believed to be due to differential thermal contraction between the PEEK polymer and the Kapton(R) film used in the heated press. This orientation is relatively insignificant when compared to the orientation that occurs when carbon fibers are present.

Quenched PPS films containing carbon fibers also exhibited extensive birefringence, and these birefringent colors were similarly partitioned by the carbon fibers (Fig. 20a). The PPS film that contained carbon fibers was crystallized as was the PEEK film but at 400 K. Again, the birefringent colors in the crystallized PPS fiber containing film were not as deep as in the amorphous state but indicated distinct polymer orientation with respect to the embedded carbon fibers (Fig. 20b).

Fig. 20

PPS

a

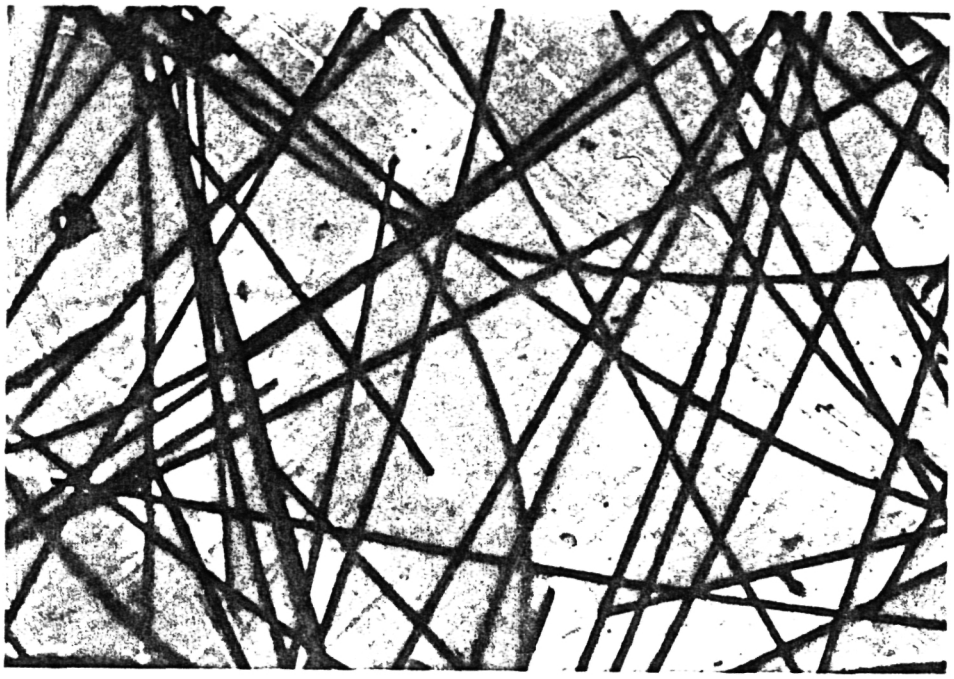

Quenched-amorphous PPS film with carbon fibers.

b

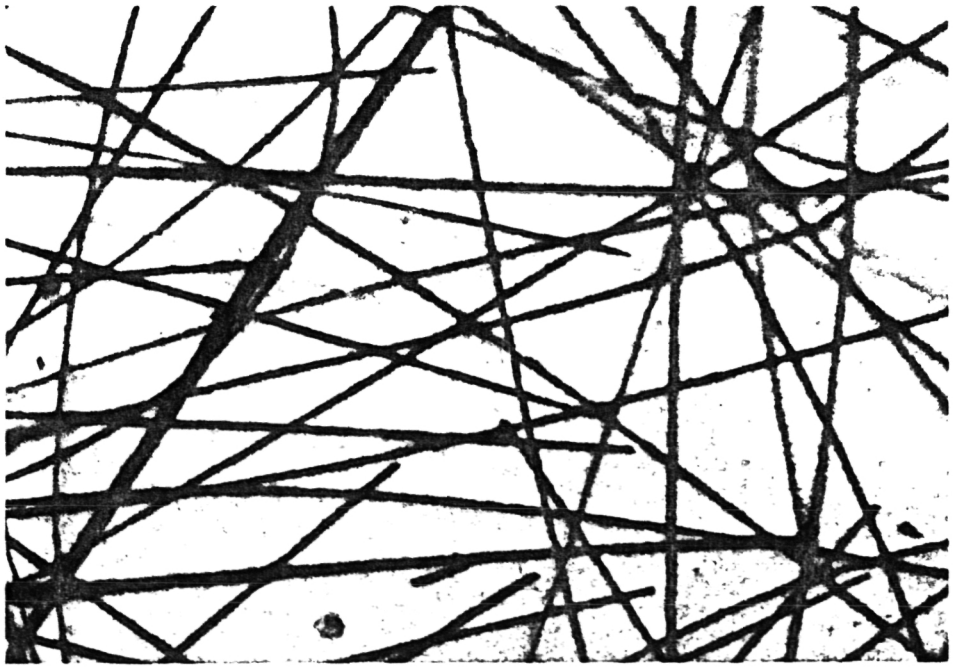

The above film crystallized at 400 K.

4.0 DISCUSSION

4.1 Isothermal Crystallization Rates

The composite samples containing either PPS or PEEK crystallized more rapidly than did the respective neat resin samples. Two probable effects of carbon fibers on crystallization rate are nucleation on the carbon fiber surface and enhancement of nucleation and growth rates from molecular orientation originating from differential thermal contraction between the carbon fibers and the polymer melt.

Plots of t_{max} vs. T_c for PPS show a dramatic increase in crystallization rate in the composite samples as compared to the neat resins. The differences are greater in the higher crystallization temperature range, above T_{max}, the temperature of maximum crystallization rate. This is indicative of increased nucleation in the composite samples. Crystallization rate at high temperatures is limited by nucleation rate. At lower temperatures, crystallization is diffusion controlled.

Differences in crystallization rates between neat PEEK and PEEK composite samples were not as great as in PPS. This may be expected if nucleation on the carbon fiber surface is a factor. Neat PEEK crystallizes with a higher nucleation density than does neat PPS. The effect of adding more primary nuclei to PEEK will not be as dramatic as adding more nuclei to PPS.

Photomicrographs of quenched PEEK and PPS films containing carbon fibers clearly demonstrate molecular orientation caused by differential thermal contraction between fibers and polymer. The orientation remained upon subsequent crystallization. This indicates that orientation may play a major role in the increased crystallization rates of the composites at lower temperatures where crystallization is diffusion controlled. The orientation may position the polymer molecules so that they may enter a growing crystal more rapidly, thus increasing the crystallization rate. Orientation will lower the entropy of the melt, thereby increasing the effective degree of supercooling. This can also increase crystallization rate.

Orientation in high temperature crystallizations of the composite samples is also likely to increase crystallization rate. Orientation is well known to increase crystallization rates of many polymers [27,28]. Further, orientation from either differential thermal contraction or mechanical stress can greatly increase the activity of heterogeneous nuclei in polypropylene [29,30]. In the high temperature crystallizations of the composites, orientation and nucleation on carbon fiber surfaces may interact synergistically to increase crystallization rate. The entropic effect on the melt, cited above, can also directly enhance nucleation rates by increasing the effective degree of undercooling [31].

4.2 Crystallization Kinetics - PPS

The Avrami exponents obtained for the neat PPS and PPS composites do not elucidate the nature of the effect of carbon fibers on the crystallization of PPS. The NASA GD441 composite samples gave exponents that were slightly higher than did the neat PPS resin, but the Phillips 58306 composite samples gave exponents below those of both the neat resin and the NASA composite. It is possible that the lower exponents found in the Phillips composite are indicative of greater heterogeneous nucleation, but this is contradicted by the slower crystallization rates found for the Phillips composite compared to those of the NASA composite.

The differences in crystallization kinetics between the NASA and Phillips composites may well be due to different resin formulations. The PPS in the Phillips composite may contain molecular branching or may be of higher molecular weight than that in the NASA samples. This could, in turn significantly slows the crystalline linear growth rate so as to reduce the bulk crystallization rate in spite of a greater heterogeneous nucleation rate. Another possibility is that nucleation kinetics were the same for both the NASA and Phillips composites, but a difference in the PPS resin used in the Phillips composite altered crystalline growth morphology so as

to reduce the number of lineal dimensions in which a crystallizing particle grew. Reducing the number of lineal growth dimensions will reduce the Avrami exponent and can also reduce the bulk crystallization rate.

4.3 Crystallization Kinetics - PEEK

The values of Avrami exponents obtained from high temperature isothermal crystallizations of neat PEEK were much higher than the values of 3 to 4 commonly found in most crystallizable polymer systems. Neat PEEK yielded exponents ranging in most cases from 5 to 7. Reasons for the presence of such high exponents are unclear, but it can be demonstrated that they can arise from a branched growth morphology or apparent accelerating lineal growth rates.

Nucleation density in PEEK pertaining to the initiation of new spherulitic growth centers is very high and, therefore, the sizes of its spherulites are very small. For this reason it may be necessary to consider a transitional morphology which consists of an aggregate of polymer crystallites that have not yet assumed the familiar growth habit of a spherulite. Sheathlike bundles of crystallites are known to be precursors to the more familiar spherulites [32], however, the peculiar geometry of these bundles has not been considered as a factor in determining crystallization rates. It may be that in the

crystallization of PEEK, these structures assume an importance in crystallization kinetics that has not been seen in other systems. Electron micrographs of developing spherulites grown from dilute solutions, obtained by Lovinger and Davis, exhibit growth through a branching fibrillar morphology instead of growth from stacked sheetlike lamellae commonly found in crystalline polymers [13]. Initial growing branches may grow unrestricted in direction until they fill surrounding space and impinge, forming the common spherulite geometry. From this point on, growth is restricted in the radial direction of the resultant spherulite.

An analogy may br found in the development of a bush. It begins with a few branches, fills in with age, and finally attains a spherical shape. Transition from branched growth geometry to spherical will give an apparent non-constant lineal growth rate if a spherical shape for the particles of the developing phase is assumed.

The suggested development of a PEEK spherulite is schematically represented in Fig. 21. The spherulite begins as a crystalline axialite with growth occurring at its ends in the form of branching fibrils. If lineal growth rate is constant, then the length of the growth radial (r) will be proportional to time. The mushrooming effect brought about by the branching will cause the arc length (a) of the growth surface to increase

Fig. 21

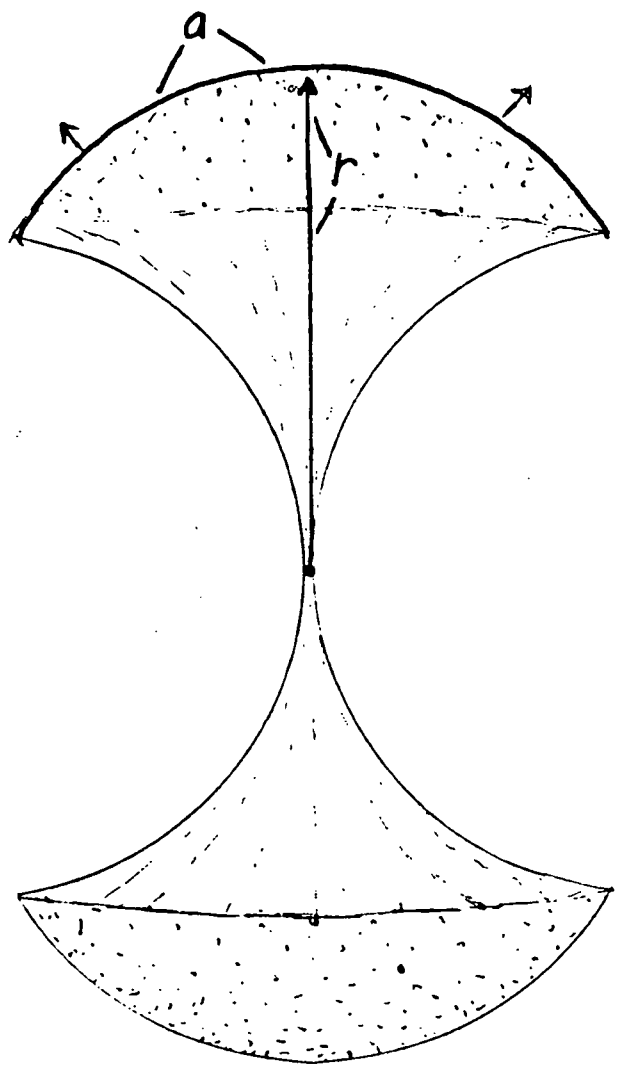

with the growth radial (r) in an exponential fashion and, therefore, (a) will also increase with time in an exponential fashion. The geometry of the growing spherulite will not be constant with time during this induction period. The ratio of growth surface area with r^2 will be increasing with time, and the resulting Avrami exponent will be a function of the increasing growth surface due to changing geometry in addition to increasing growth surface derived from increasing radius. In common spherulite growth schemes, the growth geometry is assumed to be constant (a sphere; as the name implies) and a growth surface arc length will increase exponentially with time only if lineal growth rate is accelerating. If conversion in neat PEEK consists of growth which is of the branching type suggested above, then the experimental PEEK Avrami exponents should be approximated if growth kinetics are derived for a sphere with accelerating lineal growth rates. The following derivation is generated by recasting equations 1.2 - 1.6 using accelerating lineal growth rates.

When nucleation is a random process (homogeneous case) the number of nuclei to form in the time period t may be given by

$$n = NM_o t \quad \text{or} \quad dn = NM_o dt \tag{4.1}$$

where n is the number of nuclei, and M_o is the total mass of the crystallizing material, and N is the nucleation rate with dimensions $[n.mass^{-1}.t^{-1}]$.

If the lineal growth rate experiences constant acceleration, then the radius of a growing spherulite at any time t will be given by

$$r = (a/2)(t - t_i) \tag{4.2}$$

where a is lineal acceleration in distance/time squared, and t_i is the time at which the spherulite was nucleated.

The change in crystalline mass (dM_c) with respect to time may be given by

$$dM_c = NM_o dt_i(\pi a^3(t - t_i)^6 \rho_c/6 \tag{4.3}$$

where ρ_c is the density of the crystalline phase.

The total crystalline mass (M_c) at time t is obtained by integration of (4.3) between the limits of $t_i = 0$, and $t_i = t$ which yields

$$M_c = M_o(1/42)(\pi N a^3 \rho_c)t^7 \tag{4.4}$$

Dividing by M_o and combining the constants in the parentheses

into one constant gives

$$M_c/M_o = k''t^7 \qquad (4.5)$$

The Avrami exponent in equation (4.5) is 7 (or 6 if nucleation is heterogeneous) which is consistent with those found with neat PEEK.

Avrami exponents calculated for the PEEK composite samples were found to be much lower than those in neat PEEK. This suggests that nucleation may be occurring on the carbon fiber surfaces. Nuclei formed on the fiber surface may be thicker and occur with greater areal density than those formed in the bulk, thus restricting their growth direction normal to the plane of the fiber surface. This would result in a constant growth geometry very early in the crystallization, thereby, eliminating contributions to the Avrami exponent from changing geometry of the growing species as crystallization progressed.

4.4 Tm* vs. Tc Analyses - PEEK and PPS

In DSC thermograms generated for T_m* vs. T_c analyses, dual endotherms were observed for all samples. As crystallization temperature increased, the positions of the primary melting remained fairly constant until an increase began at higher crystallization temperatures. Inherent heterogeneities present

in the neat polymers, as well as in the composites, may be responsible for the constancy of the primary peak positions at the lower crystallization temperatures. Heterogeneities may initiate the growth of thick crystallites relative to the minimum thickness required for thermal stability at the lower temperatures.

The slightly higher melting temperatures in neat PPS and PPS composite samples at the lowest crystallization temperatures were possibly due to melting-recrystallization phenomena occurring during DSC heating scans, and not from the states they attained during the isothermal crystallizations that preceded heating. The phenomenon could start when less thermally stable crystallites melt in the early part of the heating scan. That molten material would then recrystallize and remelt as the DSC scan progresses.

The primary melting occurred at higher temperatures for the composite than in the neat polymer for both PEEK and PPS systems. This is probably due to nuclei forming in the composites which are thicker in the chain direction than those forming in the neat polymer. The cause for thicker nuclei in the composites may be nucleation on the carbon fiber surfaces or from orientation of the polymer melt through differential thermal contraction. One must suppose that energetic considerations are overriding in the formation of thicker nuclei, since

entropic contributions would oppose such an occurrence. Such nuclei will grow into thicker lamellae than would otherwise form, and could, under favorable circumstances, nucleate additional thick lamellae growing outwardly in the spherulite radial direction. This is reasonable considering the findings of Lovinger and Davis, in which PEEK and PPS lamellae were found to grow as fibrils with growth directions parallel to the spherulite radii [13,18].

The thermal stabilities of secondary crystallites formed at lower crystallization temperatures did not level off with T_c. Their melting points increased linearly with crystallization temperature giving a slope of about 0.9. If heterogeneities are responsible for the leveling off of the primary peak positions, then, apparently the positions of these low temperature peaks are unaffected by the presence of heterogeneities. This is consistent with the finding that the more thermally stable crystals representing the primary peak form first in both PEEK and PPS crystallizations. Any heterogeneous nuclei initially present, other than ones forming on existing crystallite surfaces, must immediately be utilized by the formation of the higher melting crystals. One can surmise that these less stable crystals form in locations that are beyond the influence of carbon fibers and that their morphology is influenced more by crystallization temperature than by carbon fiber or other

surfaces. This is apparently why the presence of carbon fibers has no affect on the secondary peak positions.

The secondary crystals form from polymer chains held in constrained, possibly somewhat extended configurations through entrapment of chain segments in the primary crystals. Indeed, some secondary crystallites may form from chains in the melt that are constrained by previously formed secondary crystallites. The entropy changes associated with crystallizing and melting the secondary crystals will not be as great as in the melting of unconstrained chains, since in the melt, chains which are restricted will have a lower number of possible configurations available to them. Thus T_m of the secondary crystallites will be increased as shown by $T_m = \Delta H/\Delta S$. The effectively increased supercooling of the secondary crystallites will encourage their crystallization at temperatures above which they would normally crystallize. However, as the population of secondary crystals begin to melt, constraints are relaxed on the amorphous chains associated with the remaining secondary crystallites. This would lower the melting temperatures of the remaining secondary crystallites and lead to a relatively sharp melting peak for them rather than a broad melting continuum that might be expected for crystallites that were formed from a melt that is progressively becoming depleted of crystallizable sequences. Thus, the release of constraints on the remaining

secondary crystallites as the earlier ones melted could lead to a cascade of melting. We may further speculate that in the case of the primary crystallites, morphologies change in a systematic way with increasing crystallization temperature so that constraints upon the remaining crystallizable chains increase in the amorphous phase and yield the observed change in thermal stability of the secondary crystals. Thus, this line of thought suggests that the high slope of the secondary peak position vs. crystallization temperature indicates that secondary crystallization occurs in a restricted melt. Applying equation (1.20) to the secondary peak positions gives β a value of about 0.55 indicating that the population of crystals responsible for the secondary peak (secondary crystals) form with thicknesses close to the minimum required for thermal stability.

The case for the crystallite thickness, $\underline{l}$, being closely associated with the critical thickness of the nucleus formed during two-dimensional nucleation, $\underline{l}_2^*$, may also be relevant. Equation (1.22) shows that if $\underline{l}$ grows slightly larger than $\underline{l}_2^*$, i.e., $\beta > 1$, then the crystal will be thermodynamically stable in that it will melt at $T > T_c$. The slopes of close to 1 in our T_m^* vs. T_c plots could be indicative of such a two-dimensional process as is suggested by equation (1.22).

Apparently, the secondary crystallization occurs in amorphous regions which have been rigidified [7] by surrounding higher

melting crystals. The secondary crystals grow slowly and to the minimum thickness required to form stable crystals in the restricted amorphous material. This is consistent with the study of Cheng et al. of crystalline PEEK in which a rigid amorphous fraction was identified [7].

BIBLIOGRAPHY

(1) R.J. Diefendorf and E. Tokarsky, Polym. Eng. and Sci., 15, 150 (1975).

(2) T.E. Attwood, P.C. Dawson, J.L. Freeman, L.R.J. Hoy, J.B. Rose, and P.A. Staniland, Polym. Prepr., 20, 191 (1979).

(3) T.E. Attwood, P.C. Dawson, J.L. Freeman, L.R.J. Hoy,, J.B. Rose, and P.A. Staniland, Polymer, 22, 1096 (1981).

(4) M.T. Bishop, F.E, Karasz, and P.S. Russo, Macromolecules, 18, 86 (1985).

(5) D.P. Jones, D.C. Leach, and D.R. Moore, Polymer, 26, 1385 (1985).

(6) S. Don, P. Cebe, S. Chung and A. Gupta, unpublished results.

(7) S.Z.D. Cheng, M.Y. Cao, and B. Wunderlich, Macromolecules, 19, 1868 (1986).

(8) A.J. Lovinger, D.D. Davis, and F.J. Padden, Polymer, 26, 1595 (1985).

(9) P.J. Boeke, "Modern Plastics Encyclopedia, 1981-1982", McGraw-Hill, New York, NY, p.78.

(10) R.S. Shue, J.H. Walker, J.S. Dix, and D.G. Brady, Plastics Engineering, 39, No.4, 37 (1983).

(11) D.J. Blundell and B.N. Osborn, Polymer, 24, 953 (1983).

(12) P. Cebe and S. Hong, Polymer, 27, 1183 (1986).

(13) A.J. Lovinger and D.D. Davis, Macromolecules, 19, 1861 (1986).

(14) Y. Lee and R. Porter, Polym. Eng. and Sci., 26, 633 (1986).

(15) F.N. Cogswell, 28th National SAMPE Symposium, April 12-14, 1983, p.528.

(16) D.J. Blundell, J.M. Chalmers, M.W. Mackenzie, and W.F. Gaskin, SAMPE Quarterly, 16(4), 22 (1985).

(17) D.G. Brady, J. Appl. Polym. Sci., 20, 2541 (1976).

(18) A.J. Lovinger and F.J. Padden, Bull. Am. Phys. Soc., 27, 259 (1982).

(19) M. Avrami, J. Chem. Phys., 7, 1103 (1939); ibid., 8, 212 (1940); ibid., 9, 177 (1941).

(20) L. Mandelkern, "Crystallization of Polymers", McGraw-Hill, New York, 1964, p. 224.

(21) J.D. Hoffman and J.J. Weeks, J. Res. Nat. Bur. Standards, V.66A, 13 (1961).

(22) L. Mandelkern, "Crystallization of Polymers", McGraw-Hill, New York, 1964, p. 321.

(23) A.P. Gray, in "Analytical Calorimetry", Ed. R.S, Porter and J.F. Johnson, Plenum Press, New York, 1968, p. 209.

(24) E. Pella and M. Nebuloni, J. Thermal Anal., 3, 229, 1971.

(25) M.H. Theil and T.W. Towell, Thermal Analysis of Composite Samples Made With PEEK Thermoplastic Resin, unpublished results, 1985.

(26) T. Mertha, Private Communication, Phillips Petroleum Co., Bartlesville, OK.

(27) L. Mandelkern, "Crystallization of Polymers", McGraw-Hill, New York, 1964, p. 166.

(28) A. Ziabicki, Colloid & Polymer Sci., 252, 207 (1974).

(29) M.G. Hudson and W.J. McGill, J. Polym. Sci., Polym. Chem. Ed., 22, 3571 (1984).

(30) D.G. Gray, J. Polym. Sci., Polym. Lett. Ed., 12, 645, (1974).

(31) L. Mandelkern, "Crystallization of Polymers", McGraw-Hill, New York, 1964, chap. 8.

(32) H. D. Keith and F. J. Padden, Jr., J. Appl. Phys., 34, 2409 (1963).

APPENDIX

A. PPS - Isothermal Crystallization Experiments

B. PEEK - Isothermal Crystallization Experiments

Explanation of Abbreviations

Cryst. frac.: Degree of crystallinity from DSC

Corr.: Correlation coefficient

Thermal history

Ov: Heated first in oven

1st, etc.: Number of prior DSC melting and crystalliztion cycles undergone by sample

n: Avrami equation expoent

PPS - Isothermal Crystallization Experiments

File #	Sample	T_c (K)	Mass (mg)	Resin frac.	Thermal History	Area (cal/g)	Cryst. frac.	t_{max} (min)	n	Corr.
01213	neat	400	13.21	1.00	0v	6.19	0.26	2.09	—	—
01214	neat	395	11.04	1.00	0v	5.07	0.21	4.08	—	—
01215	neat	490	5.98	1.00	5min-600	8.13	0.34	4.07	—	—
01216	neat	490	6.97	1.00	5min-600	7.55	0.32	4.41	3.08	0.9998
01217	neat	495	9.14	1.00	1st	9.07	0.38	6.84	—	—
01218	neat	485	9.14	1.00	2nd	9.29	0.39	2.87	3.18	0.99999
01219	neat	500	9.14	1.00	3rd	9.42	0.39	11.13	3.08	0.9998
01220	neat	505	9.14	1.00	4th	5.61	0.23	20.64	—	—
01221	GD441	495	25.65	—	0v, 1st	4.07	—	1.86	—	—
01222	GD441	500	25.65	—	0v, 2nd	4.47	—	2.77	3.28	0.9987
01223	GD441	505	25.65	—	0v, 3rd	4.58	—	4.39	—	—
01224	GD441	390	25.52	—	0v	2.53	—	3.72	—	—
01225	GD441	505	25.52	—	0v, 1st	4.66	—	3.80	—	—
01226	GD441	500	25.52	—	0v, 2nd	4.56	—	2.69	3.28 (5.23)	0.9993 (0.9940)
Y	GD441	495	25.52	—	0v, 3rd	4.61	—	1.86	3.43	0.9843
01227	GD441	510	21.10	—	0v, 1st	4.06	—	6.75	2.90	0.9992
01228	GD441	385	17.76	—	0v	1.51	—	9.71	—	—

PPS - Isothermal Crystallization Experiments (cont.)

File #	Sample	T_c (K)	Mass (mg)	Resin frac.	Thermal History	Area (cal/g)	Cryst. frac.	t_{max} (min)	n	Corr.
01229	GD441	395	22.36	—	0v	2.79	—	1.78	3.74	0.9997
01231	GD441	490	22.36	—	0v, 2nd	4.42	—	1.49	3.38	0.9994
01232	GD441	485	22.36	—	0v, 3rd	4.32	—	1.14	—	—
01233	neat	405	9.71	1.00	0v	6.05	0.25	1.04	—	—
01234	neat	475	9.71	1.00	0v, 1st	9.06	0.38	1.62	3.09	0.9993
01239	GD441	510	15.53	—	0v, 1st	4.14	—	7.48	3.10 (4.29)	0.9997 (0.9984)
01241	GD441	505	15.53	—	0v, 3rd	4.24	—	4.50	3.11	0.9997
01242	neat	390	17.09	1.00	0v	4.33	0.18	8.76	3.96 (5.36)	0.9995 (0.9982)
01243	neat	395	10.82	1.00	0v	5.01	0.21	3.82	—	—
01244	neat	405	9.00	1.00	0v	5.78	0.24	1.16	—	—
01245	GD441	400	21.98	—	0v	2.72	—	1.11	—	—
01246	GD441	385	27.12	—	0v	1.99	—	9.60	3.99	0.99999
01248	58306	500	19.95	—	0v	3.94	—	3.86	—	—
01249	GD441	500	24.00	—	1st	4.54	—	2.21	3.37	0.9997
01250	GD441	505	24.00	—	2nd	4.45	—	3.67	—	—
01251	58306	490	15.98	—	1st	4.14	—	1.90	—	—
01252	58306	500	15.98	—	2nd	4.16	—	2.59	2.66	0.99999

PPS - Isothermal Crystallization Experiments (cont.)

File #	Sample	T_c (K)	Mass (mg)	Resin frac.	Thermal History	Area (cal/g)	Cryst. frac.	t_{max} (min)	n	Corr.
01253	58306	500	15.98	—	3rd	4.49	—	4.30	2.59	0.9988
01254	58306	505	15.98	—	4th	3.97	—	6.06	—	—
01255	neat	485	8.86	1.00	1st	8.93	0.37	2.45	3.04 (3.89)	0.9992 (0.9986)
01256	neat	480	8.86	1.00	2nd	8.92	0.37	1.79	3.26	0.9984
01257	GD441	515	19.55	—	Ov, 1st	3.82	—	11.40	3.38	0.9989
01258	F-film	495	4.54	—	press,1st	6.51	—	3.68	—	—
01259	F-film	490	4.54	—	press,2nd	5.74	—	2.64	—	—
01260	F-film	495	4.54	—	press,3rd	5.23	—	4.02	—	—
01261	F-film	490	4.54	—	press,4th	5.29	—	2.84	—	—
01262	n-film	490	4.43	1.00	press,1st	9.36	0.39	3.12	—	—
01263	n-film	490	4.43	1.00	press,2nd	9.57	0.40	3.13	—	—
01264	n-film	495	9.24	1.00	press,1st	10.10	0.42	4.27	—	—
01265	n-film	495	9.24	1.00	press,2nd	8.56	0.36	4.51	—	—

PEEK - Isothermal Crystallization Experiments

File #	Sample	T_c (K)	Mass (mg)	Resin frac.	Thermal History	Area (cal/g)	Cryst. frac.	t_{max} (min)	n	Corr.
01401	CD432 #5	570	20.12	0.33	1st	3.52	0.34	0.77	—	—
01402	CD432 #5	590	20.12	0.33	2nd	3.74	0.36	6.47	3.51	0.9999
01403	CD432 #5	580	20.12	0.33	3rd	3.48	0.34	1.92	3.69	0.9995
01404	neat	580	8.54	1.00	1st	8.15	0.26	3.43	—	—
01405	neat	570	8.54	1.00	2nd	8.69	0.28	1.20	7.11	0.9993
01406	CD433 #6	590	25.88	—	1st	3.81	—	6.61	3.75	0.9989
01407	CD433 #6	580	25.88	—	2nd	3.74	—	2.02	3.81	0.9998
01408	CD433 #6	585	25.88	—	3rd	3.65	—	3.95	—	—
01409	neat	580	9.02	1.00	1st	8.85	0.28	3.27	5.77	0.9998
01410	neat	575	9.02	1.00	2nd	8.38	0.27	1.99	7.14	0.9977
01411	neat	570	9.02	1.00	3rd	9.29	0.30	1.21	6.98	0.9985
01412	CD432 #4	440	24.80	0.32	0v	1.68	0.17	0.96	—	—
01413	CD432 #4	595	24.80	0.32	0v, 1st	2.74	0.28	15	—	—
01414	CD433 #5	430	31.60	0.34	0v	1.36	0.13	8.55	3.38	0.9999
01416	CD433 #6	575	25.88	—	4th	3.69	—	1.49	—	—
01417	CD433 #6	575	25.88	—	4th,680K	3.75	—	1.50	—	—
01418	CD432 #5	432.5	20.12	0.33	3rd,0v	1.31	0.13	7.50	—	—
01419	neat	432.5	8.61	1.00	press	—	—	7.60	—	—

PEEK - Isothermal Crystallization Experiments (cont.)

File #	Sample	T_c (K)	Mass (mg)	Resin frac.	Thermal History	Area (cal/g)	Cryst. frac.	t_{max} (min)	n	Corr.
01420	neat	435	10.10	1.00	press	3.74	0.12	2.19	—	—
01421	neat	590	8.85	1.00	1st	—	—	15.8	—	—
01422	GD433 #4	430	29.54	0.34	0v	—	—	7.22	—	—
01423	GD433 #8	432.5	28.45	—	0v	1.02	—	4.33	4.71	0.9975
01424	GD432 #6	435	24.77	0.33	0v	1.35	0.13	2.27	3.01	0.9996
01425	GD433 #5	435	31.60	0.34	0v,0v	1.03	0.10	1.98	4.41	0.9975
01426	GD432 #6	437.5	20.12	0.33	3rd,0v,0v	1.60	0.16	1.35	—	—
01427	GD432 #3	440	21.90	—	0v	1.82	—	0.84	—	—
01428	GD432 #4	432.5	24.80	0.32	0v,1st,0v	—	—	3.46	—	—
01429	neat	430	9.21	1.00	press	3.54	0.11	19.1	4.20	0.9999
01430	neat	432.5	7.09	1.00	press	5.09	0.16	7.90	3.61	0.99999
01431	neat	435	9.87	1.00	press	4.57	0.15	3.69	4.51	0.99997
01432	neat	437.5	8.16	1.00	press	4.37	0.14	2.45	5.27	0.9998
01433	neat	580	8.16	1.00	press,1st	8.58	0.28	4.13	—	—
P585	neat	585	11.11	1.00	1st	—	—	5.95	—	—
01601	APC-1	580	25.11	—	1st	3.75	—	2.51	3.44	0.9989
01602	APC-1	575	25.11	—	2nd	3.51	—	1.71	3.64	0.9982
01603	APC-1	585	25.11	—	3rd	2.36	—	4.85	4.29	0.9974